



TAMPEREEN TEKNILLINEN YLIOPISTO
TAMPERE UNIVERSITY OF TECHNOLOGY

DEEPAK SANKAR AMARIPADATH
EFFECTS OF DIFFUSE RADIATION TO THE OPERATION OF
PHOTOVOLTAIC POWER PLANTS

Master of Science thesis

Examiner: prof. Seppo Valkealahti
Examiner and topic approved by
the Faculty Council of the Faculty
of Electrical Engineering on 3rd
December 2014

ABSTRACT

TAMPERE UNIVERSITY OF TECHNOLOGY

Master's Degree Programme in Electrical Engineering

AMARIPADATH, DEEPAK SANKAR: Effects of diffuse radiation to the operation of photovoltaic power plants

Master of Science Thesis, 43 pages, 1 Appendix page

May 2015

Major: Smart Grids

Examiner: Professor Seppo Valkealahti

Keywords: PV power plants, solar irradiance, diffuse radiation

Despite the large potential, only a fraction of solar energy reaching earth's surface is utilized in power production. In recent years the number of photovoltaic power plants in Finland has increased. It is important to learn how different components of solar radiation affect the working of PV power plants. The diffuse radiation component of solar irradiance is relatively difficult to harvest when compared to global and direct radiation. Thus a fraction of solar radiation is lost during energy harvesting. Although it seems like the diffuse radiation only forms a small fraction of total radiation it has a significant effect on working of PV power plants.

Thus it was important to study the radiation profiles from the test location in Tampere University of Technology, Tampere, Finland. The annual variations in solar radiation profiles for past three years were studied to determine the variations in amount of solar radiation received per year. Also seasonal variations were studied to understand how the climatic variables can influence solar irradiance. The effects of cloud variation were also studied by analyzing daily radiation profiles for clear sky and cloudy sky days. The effective ways to harvest diffuse radiation were also studied.

The results showed that during winter the amount of diffuse radiation is almost equal to global radiation. The total amount of irradiance during winter is far lower when compared to summer months. Thus during winter it is important to harvest every available solar energy to ensure maximum production and efficiency. The effects of cloud percentage showed that the amount of diffuse radiation increased with increase in cloud percentage in the sky. Humidity of atmosphere had a similar effect causing increase in amount of diffuse radiation with increase in humidity content in atmosphere. Thus the studies revealed that it was important to ensure that the diffuse radiation component was also harvested by the PV power plants for maximum production and working efficiency.

PREFACE

This Thesis is submitted in partial fulfillment of Master of Science (Technology) degree in Electrical Engineering from Tampere University of Technology. It was a great opportunity to work with this topic and I was able to learn a lot from this. I would like to thank my supervisor, Prof. Seppo Valkealahti for his inspiration, guidance, time and ideas throughout the thesis. His remarkable support has helped me to make this thesis possible and fruitful.

I would also like to thank MSc. Kari Lappalainen for his guidance and support. He was readily available to help whenever I needed it. I also thank Department of Electrical Engineering, TUT for providing me with excellent laboratories, equipment's and a pleasant work environment. I also thank my family and friends for their immense support throughout the thesis. I would like to specially thank my dad for his support and encouragement for my every decision.

Tampere, 25.04.2015

Deepak Sankar Amaripadath

CONTENTS

1.	INTRODUCTION	1
2.	SOLAR ENERGY	4
2.1	Wave-particle duality	4
2.2	Black body radiation	4
2.3	Solar irradiance fundamentals	5
2.4	Factors affecting solar radiation	10
2.5	Effects of shading.....	11
3.	DIFFUSE RADIATION	13
3.1	Introduction	13
3.2	Atmospheric scattering.....	14
3.2.1	Rayleigh scattering	14
3.2.2	Mie scattering	15
3.3	Clearness and clear sky index	16
3.4	Measurement of solar radiation using empirical models	17
3.4.1	Based on sunshine hours	17
3.4.2	Based on air temperature.....	17
3.5	Direct measurement of solar irradiance	18
4.	SOLAR PV RESEARCH PLANT AT TUT.....	21
4.1	Layout.....	21
4.2	Sensors	22
4.2.1	Solar irradiance on PV modules	23
4.2.2	Diffuse and global irradiance	24
4.2.3	Temperature and humidity.....	26
4.2.4	Wind speed and direction	27
5.	RESEARCH AND ANALYSIS.....	28
5.1	Annual radiation profiles.....	28
5.2	Seasonal variation of radiation profiles.....	30
5.3	Daily variation of radiation profiles	33
5.4	Irradiance ratio and cloud distribution	36
5.5	Irradiance ratio and humidity	37
6.	CONCLUSIONS.....	39
	REFERENCES.....	41
	APPENDIX A. TUT solar photovoltaic power station test plant	44

LIST OF FIGURES

<i>Figure 2.1 Spectral intensity of black body radiation at varying temperature values based on Planck's radiation law.....</i>	<i>5</i>
<i>Figure 2.2 Air mass ratio representation.....</i>	<i>6</i>
<i>Figure 2.3 Solar spectrum.....</i>	<i>7</i>
<i>Figure 2.4 Solar window.....</i>	<i>7</i>
<i>Figure 2.5 Annual solar declination with respect to earth's equator.....</i>	<i>9</i>
<i>Figure 2.6 Earth's orbit around the sun and the angle of tilt in earth's axis around the year</i>	<i>9</i>
<i>Figure 2.7 Modification in incoming global solar radiation in earth's atmosphere.....</i>	<i>10</i>
<i>Figure 2.8 PV characteristics of a series connected string of 7 PV modules under partial shading conditions.....</i>	<i>11</i>
<i>Figure 3.1 CHP1 Pyrheliometer.....</i>	<i>19</i>
<i>Figure 3.2 CMP21 Pyranometer.....</i>	<i>20</i>
<i>Figure 3.3 Sunshine recorder</i>	<i>20</i>
<i>Figure 4.1 Section of TUT power station test plant.....</i>	<i>22</i>
<i>Figure 4.2 Solar irradiance sensor SP Lite2</i>	<i>24</i>
<i>Figure 4.3 CMP21 pyranometer with CM121C shadow ring measuring diffuse radiation.....</i>	<i>25</i>
<i>Figure 4.4 CMP22 pyranometer measuring global radiation.....</i>	<i>25</i>
<i>Figure 4.5 Temperature and humidity sensor HMP155 inside DTR503A and DTR502A radiation shields.....</i>	<i>26</i>
<i>Figure 4.6 Wind sensor WS425.....</i>	<i>27</i>
<i>Figure 5.1 Annual radiation profile in Hervanta, Tampere for average daily values during 2014.....</i>	<i>28</i>
<i>Figure 5.2 Annual global radiation profile comparison using average daily values in Hervanta, Tampere during 2012, 13 and 14.....</i>	<i>29</i>
<i>Figure 5.3 Annual diffuse radiation profile comparison using average daily values in Hervanta, Tampere during 2012, 13 and 14.....</i>	<i>30</i>
<i>Figure 5.4 Irradiance profile for average daily values during August 2014 in Hervanta, Tampere.....</i>	<i>31</i>
<i>Figure 5.5 Irradiance profile for average daily values during February 2014 in Hervanta, Tampere.....</i>	<i>32</i>
<i>Figure 5.6 Global radiation profile comparison for average daily values during February and August 2014 in Hervanta, Tampere</i>	<i>32</i>
<i>Figure 5.7 Diffuse radiation profile comparison for average daily values during February and August 2014 in Hervanta, Tampere</i>	<i>33</i>
<i>Figure 5.8 Radiation profile for clear sky day on August 5th, 2014 in Hervanta, Tampere.....</i>	<i>34</i>
<i>Figure 5.9 Cloud percentage profile for August 5th, 2014 in Hervanta, Tampere</i>	<i>34</i>

Figure 5.10 Radiation profile for cloudy day on August 8th, 2014 in Hervanta, Tampere	35
Figure 5.11 Cloud percentage profile for August 8th, 2014 in Hervanta, Tampere	35
Figure 5.12 Humidity comparison profile for test days August 5th and 8th, 2014 in Hervanta, Tampere	36
Figure 5.13 Average daily ratio of diffuse and global irradiance and cloud percentage during August, 2014 in Hervanta, Tampere	37
Figure 5.14 Average daily ratio of diffuse and global irradiance and humidity percentage during August, 2014 in Hervanta, Tampere	38
Appendix A. TUT solar photovoltaic power station test plan	44

LIST OF SYMBOLS AND ABBREVIATIONS

Symbols

E_P	Energy of photon
h	Planck's constant
ν	Frequency
λ	Wavelength
G_λ	Spectral intensity
K	Boltzmann's constant
T	Temperature
h_s	Height of elevation
φ	Latitude
δ	Solar declination
σ	Cross section of scattering materials
N	Density of molecules
I	Intensity
I_o	Initial intensity
α	Polarizability
K_T	Ratio of measured values of global radiation over extraterrestrial radiation
K_d	Ratio of measured values of diffuse radiation over extraterrestrial radiation
K_D	Ratio of measured values of direct radiation over extraterrestrial radiation
K_t	Clearness index
K_c	Clear sky index
G_h	Global radiation on horizontal surface
I_0	Extraterrestrial radiation
ϵ	Eccentricity correction factor
G_P	Monthly mean of average daily solar irradiance on a horizontal surface
G_O	Monthly mean of average daily extraterrestrial irradiance on a horizontal surface
ω_s	Angle of mean sunrise hour

Abbreviations

USDE	United States Department of Energy
NASA	National Aeronautics and Space Administration
NASDA	National Space Development Agency
TUT	Tampere University of Technology
PV	Photovoltaic
BP	British Petroleum
DC	Direct Current
AC	Alternating Current

MATLAB	Matrix Laboratory, an interactive program for numerical computing and visualization
<i>AM</i>	Air Mass ratio
<i>WMO</i>	World Meteorological Organization
<i>WRR</i>	World Radiometric Reference
<i>WRC</i>	World Radiation Center

1. INTRODUCTION

Since the beginning of mankind energy has been one of the most important resources used for development and economic boom. It is estimated that by the year 2050, the global economic output will become 3 to 5 times we have today and 10 to 15 times by the year 2100 (Jayakumar 2009). The availability of energy is a factor which can directly influence the growth of global economy. Finding a clean, efficient, environment friendly and economical source of energy is a primary target to achieve better productivity and economic growth. The increase in use of fossil fuels has led to environmental degradation as well as depletion in its reserves.

The solar energy incident on earth's surface is estimated to a value of $1.5 \cdot 10^{18}$ kWh/year. This value is about 10,000 folds of current global power consumption. The solar energy constant from sun is roughly estimated to a value of 1.373 kW/m^2 . (Jayakumar 2009) The efficient utilization of solar energy available plays an important role here. Global solar radiance can be divided into direct and diffuse radiation. Scattering is one of the main reasons for forming diffuse radiation (Chou, Suarez 1999). Solar energy is a natural, renewable source of energy which is available to most parts of the world. Solar cells are devices which are widely used to convert solar energy in to electrical energy and this technology is known as solar photovoltaics. The amount of solar energy converted to electrical energy by the solar cell depends on the surface area, type, efficiency and light intensity.

The discovery of photovoltaic effect by Edmond Becquerel paved path for the development of photovoltaic systems as we see today. This was followed by the development of discovery of photoconductivity of selenium in 1873 by Willoughby Smith. In 1916, Robert Millikan became the first scientist to provide experimental proof for photovoltaic effect. The photovoltaic technology was born in United States in 1954 when Silicon photovoltaic cell was developed at Bell Labs by Daryl Chapin, Calvin Fuller and Gerald Pearson. It was the first solar cell which could produce enough power from solar energy to run electrical equipment's of everyday use. The initial efficiency of solar cell developed at Bell Telephone Laboratories was 4% and later another solar cell with 11% efficiency was developed. Photovoltaic technology reached milestones when Hoffman electronics developed Photovoltaic cells with efficiencies of 8%, 9%, 10% and 14% in 1957, 1958, 1959 and 1960, respectively. (USDE 2002)

In 1961, William Shockley and Hans Queisser Proposed Shockley-Queisser limit, also known as detailed balance limit which defines the maximum theoretical power conversion efficiency of single pn junction solar cells. The experiments were conducted by

observing electrical energy produced per incident photon. The experiments also took into consideration energy loss due to black body radiation, recombination of electrons and holes in the cell and spectrum losses from the radiations. The experimental results proposed that maximum conversion efficiency of a single pn junction solar cell with a bandgap of 1.4 eV and solar radiation modelled similar to 6000 K blackbody radiation was placed around 33.7%. (Shockley, Queisser 1961) In 1972, Institute of energy conversion was established at University of Delaware which became centre for photovoltaic research in next years. In recent year's government agencies like NASA, USA and NASDA, Japan has been working on developing PV systems for using them in space shuttles. Also companies like Sandia national laboratories, BP solarex, Automation tooling systems etc. have been conducting research associated to the field of photovoltaic systems. (USDE 2002)

The main benefits of solar energy are environmental benefits due to lower amount of emissions compared to non-renewable sources of power production like fossil fuels. This decrease in emissions directly decreases the risk of global warming and climate change. This also in turn decreases the health issues due to air pollution. The studies conducted by Environmental Protection Agency shows that health issues like chronic bronchitis and other respiratory disorders were reduced due to increased air quality. (Grover 2007) The economic benefits of using solar energy include lowering cost of power production as solar energy is clean and free energy source. Thus source costs related to solar power generation is approximately zero. The economic benefits due to decreased level of greenhouse gases and other pollutants are invaluable. (Baker, Fowlie, Lemoine, Reynolds 2013)

Even though the discoveries related to PV systems were made years ago, solar energy is not utilized to its full potential till date. The main issues concerning the PV power production varies from technical issues to various health and safety hazards. The main technical issue related to PV power generation includes the variability in solar power generation depending on seasons (Baker, Fowlie, Lemoine, Reynolds 2013). Also PV systems produce DC power which has to be inverted to AC power for residential use. Another potential risk includes the effect of islanding were the portion of the whole system including load and generation source acts as a separate entity. (Larsen, Brooks, Starrs 2000) Some of the safety hazards include risk of electrocution while the system is implemented and also risk of fire hazard is more in PV systems due to this DC power production as it is difficult to extinguish a DC arc when compared to an AC arc (Larsen, Brooks, Starrs 2000). Waste disposal of manufacturing wastes and broken modules is also a challenging task as it should be handled with at most care so that it wouldn't cause any further environmental degradation. (Fthenakis 2003)

The objective of this thesis is to study the effect of diffuse radiation on working of photovoltaic systems. The measurements of global radiation and diffuse radiation are done through Kipp&Zonens pyranometers CMP22 and CMP21 with CV3 ventilation unit is

present in TUT climatic measurement system (Torres Lobera 2010). These measurements are studied using simulations in MATLAB software. The average annual variation in global solar radiation and diffuse radiation are studied through these simulations. The factors which influence these variations are determined through this process.

The structure of the thesis is as follows. Chapter 2 briefly introduce to basic concepts and principles of solar energy. Also different types of radiations, effects of climatic parameters and shading are discussed in this chapter. Chapter 3 discuss about diffuse radiation. It deals with different scattering processes which causes diffuse solar irradiance. Mathematical modelling and measurements over horizontal and inclined surfaces are also studied here. Chapter 4 deals with the research facility available at TUT. In this chapter we discuss configuration, layout, different sensors used and automatic weather station in TUT. In chapter 5 the whole research and analysis processes done with regard to the thesis are discussed. This includes analysis of annual variation in global solar radiation and diffuse radiation. The results and effects of diffuse radiation on working of photovoltaic systems are presented in chapter 6. Finally, the conclusions are discussed in chapter 7.

2. SOLAR ENERGY

Solar radiation or light is normally perceived as an electromagnetic wave which travels from point of origin, which is sun to point of observation. The frequency of wave or its wavelength determines the color of the light. The interpretation of photoelectric effect by Albert Einstein in 1905 gave an insight that solar radiation is just not a wave but also has particle nature. (Hummel 2011) There are various principles which govern the pattern of solar radiation which are discussed in this chapter.

2.1 Wave-particle duality

Wave-particle duality of solar radiation was been strongly argued by Albert Einstein through his interpretation of photoelectric effect in 1905. The development of quantum theory in 1901 provided support to his arguments. Even though the particle nature of light was first propose by Newton about 300 years before these developments he did not had any scientific refinement at that time to back his original ideas. (Hummel 2011) Einstein made his argument through equation for measuring energy of photon as

$$E_p = h\nu = \frac{hc}{\lambda}, \quad (2.1)$$

Where E_p is energy of photon, h is Plank's constant which is equal to $6.602 \cdot 10^{-34}$ Js, ν is frequency of the wave, c is speed of light in vacuum which is equal to $2.99792 \cdot 10^8$ m/s and λ is wavelength of light (Lappalainen 2013).

2.2 Black body radiation

Black body radiation phenomenon has played an important role in the development of quantum physics. A black body may be defined as a surface which is able to absorb all radiations of any wavelength with zero reflection. That is the absorptance value of a black body is unity or 1 (Varró 2006). In the beginning of 20th century Planck developed a formula for spectral irradiance and the formula is known as Planck's radiation law and is as follows

$$G_\lambda(\lambda, T) = \frac{2\pi hc^2}{\lambda^5 (e^{\frac{hc}{\lambda kT}} - 1)}, \quad (2.2)$$

where G_λ is spectral intensity, k is Boltzmann's constant which is equal to $1.38065 \cdot 10^{-23}$ J/K and T is absolute temperature. The black body radiation spectrum intensity for 5800 K temperature is shown in figure 2.1. It is approximately the surface temperature of sun. (Lappalainen 2013)

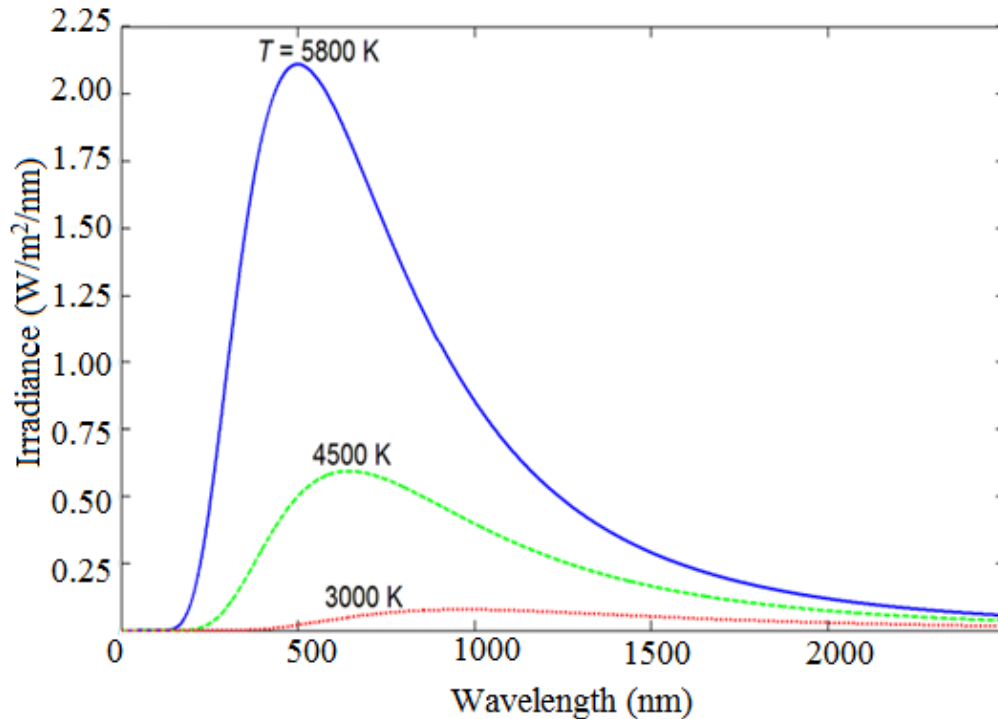


Figure 2.1. Spectral intensity of black body radiation at varying temperature values based on Planck's radiation law (Lappalainen 2013).

From figure 2.1 and equation 2.2 we can deduce that the higher the surface temperature of black body is the higher will be the spectral intensity at lower wavelengths.

2.3 Solar irradiance fundamentals

It might seem that the solar radiation from sun reaches the earth's surface and that it is a simple process. It is important to understand that there are some governing principles which influence the solar radiation from sun to earth. Some of the important principles are discussed below.

Sun is a primary source of energy for earth. As explained before, a body with temperature greater than zero radiates energy out. The surface temperature of sun is high and approximately equal to 5800 K (Lappalainen 2013). At this surface temperature a number of fusion reactions take place inside sun releasing large amount of energy. Solar irradiance is a technical term used to express the rate of electromagnetic radiation per unit area on surface of earth. Some of the main factors which cause fluctuation in rate of solar irradiance are weather conditions and position of sun. (Jayakumar 2009)

Air mass ratio can be defined as the ratio of length of path taken by solar radiation to reach earth's surface to shortest possible path. Air mass ratio is used to quantify the loss of intensity of solar radiation when it propagates through atmosphere due to absorption and reflection by dust and other particles present in the atmosphere.

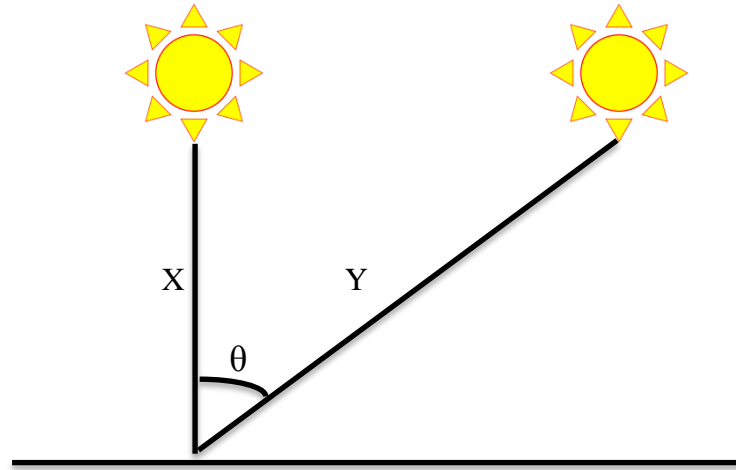


Figure 2.2. Air mass ratio representation (Riordan, Hulstrom, Myers 1990).

Figure 2.2 represent air mass ratio calculation. From the figure it is possible to calculate air mass ratio equation as

$$AM = \frac{1}{\cos \theta}, \quad (2.3)$$

where θ is the zenith angle. When the sun is positioned directly over head the value of air mass ratio is 1. (Riordan, Hulstrom, Myers 1990) The power from sun is radiated in form of a spectrum or band of electromagnetic radiations. The solar spectrum can be classified into ultraviolet, visible and infrared radiation. Ultraviolet radiation constitutes about 7% of solar spectrum. Visible radiation accounts up to 47%. The remaining 46% is infrared radiation.

Ultraviolet radiation is harmful to living cells and it is filtered out by ozone layer in atmosphere before it reaches earth's surface. Visible radiation is mainly collected by photovoltaic cells for the energy conversion process. The solar spectrum varies from a wavelength of 200 to 2400 nm. (Jayakumar 2009) Ultraviolet radiations vary from a wavelength of 250 to 400 nm. The visible radiation lies between wavelengths of 400 to 700 nm. The rest of the spectrum is made up of infrared radiations. Figure 2.3 depict the various elements in a solar spectrum.

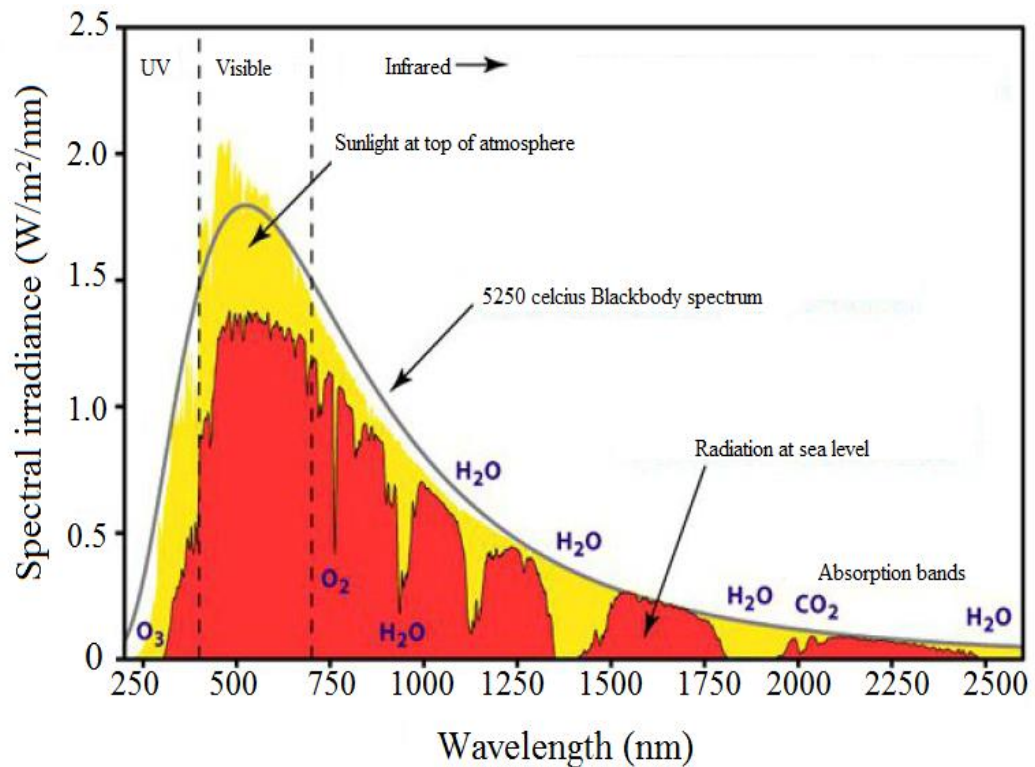


Figure 2.3. Solar spectrum (Ahola 2013).

Solar window is another important principle to be understood for designing an efficient photovoltaic system. Solar window is a specific area or location through which majority amount of sunlight passes annually (Jayakumar 2009). The positioning of solar window is important because the sun's path changes with different seasons. Sun has a different path during summer and winter and this is taken into consideration while designing the solar window.

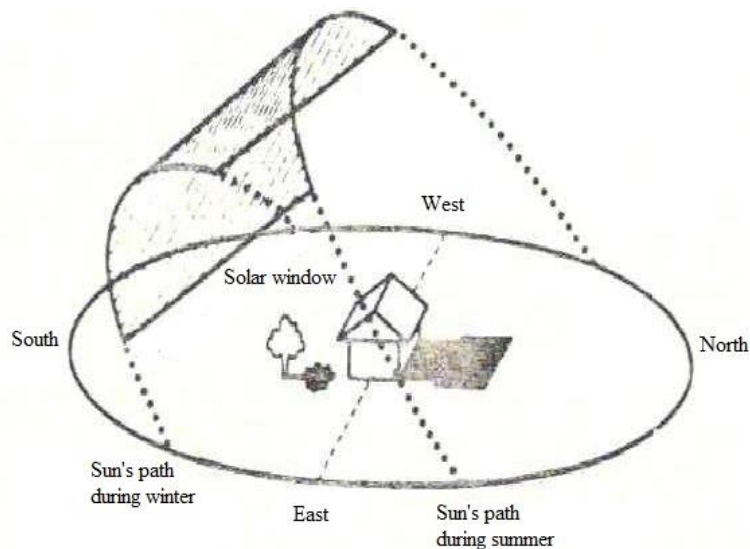


Figure 2.4. Solar window (Jayakumar 2009).

Figure 2.4 is depiction of a solar window considering the path of sun during summer and winter. Thus this window is located such that it has maximum passage of solar radiation throughout the year. Hence it is possible to position the solar panels for collecting more solar radiation as the maximum amount of solar radiation passes through the solar window.

Solar constant is defined as the amount of solar radiation energy per unit area. Solar constant is measured outside the earth's atmosphere forming a perpendicular plane to the solar radiations. One important factor to be considered while considering solar constant is that it includes all elements of solar spectrum and not only the visible spectrum of light. The value of solar constant varies within a year. It is approximately equal to 1.412 kW/m^2 during the month of January and during the month of June the value is 1.321 kW/m^2 . The main reason for this difference in values is due to varying distance between earth and sun. The annual mean value of solar constant is approximated to a value 1.366 kW/m^2 . (Jayakumar 2009)

Solar insolation is amount of solar radiation energy receive per unit area for particular amount of time. Due to movement of earth solar insolation is measured on hourly and daily basis. The hourly measurements of solar insolation data helps to identifying peak solar hours (Jayakumar 2009). As discussed before the solar insolation data's changes annually like other measurements.

One year is the time taken by earth to complete one rotation around the sun. While rotating around sun, earth rotates around its axis too. One day is counted when earth completes one rotation around its axis. The angle of declination of earth is 23.45^0 with respect to its own plane of rotation around the sun. The orientation of earth's axis is retained throughout the year. It is also to be noted that during winter angle of inclination is negative and during summer it is positive. (Häberlin 2012) We can find the height of elevation of sun from the formula

$$h_s = 90^0 - \varphi - \delta , \quad (2.4)$$

where h_s is the height of elevation of sun, φ is latitude location and δ is solar declination.

Annual solar declination values with respect to earth's equator from January 1st to December 31st are presented in figure 2.5. It can be understood that solar declination magnitude is similar during summer and winter but the sign of magnitude is positive during summer and negative during winter.

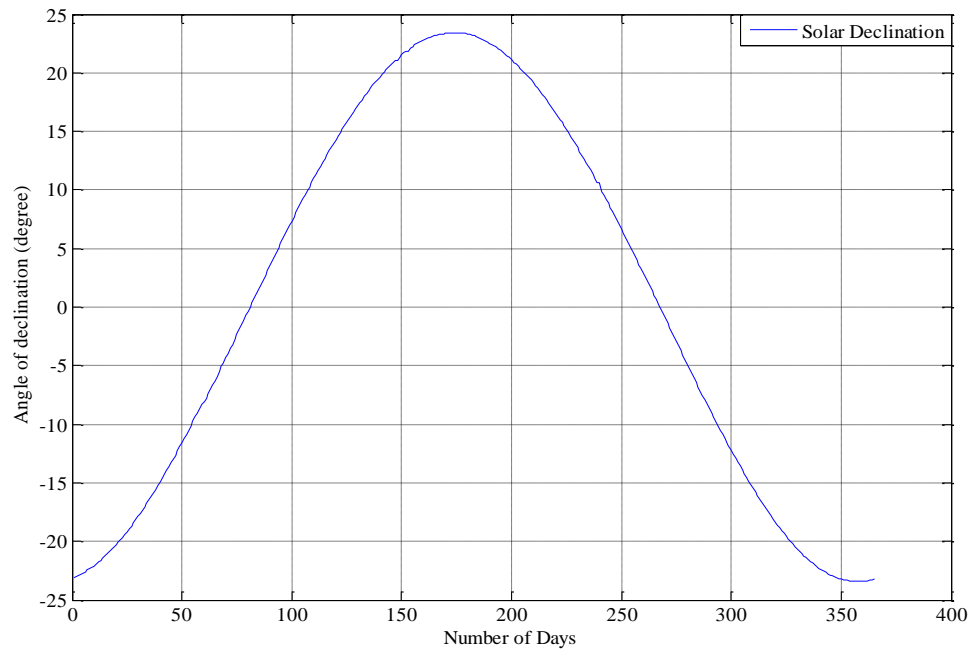


Figure 2.5. Annual solar declination with respect to earth's equator (Häberlin 2012).

The earth moves around the sun throughout the year. Hence while watching from a point on earth the sun appears to us as moving around earth. In order to use the solar energy to its maximum efficiency it is important to understand this apparent motion of sun. The maximum angle of tilt in earth's axis angle is $\pm 23.45^\circ$ (Lappalainen 2013). Considering northern hemisphere this is $+23.45^\circ$ during June 21st which is summer solstice and -23.45° during December 21st which is winter solstice. Considering southern hemisphere the winter solstice is on June 21st and summer solstice is on December 21st as the latitude value is less than 0° . The angle of declination is zero around March 21st and September 23rd at the equinoxes. (Häberlin 2012)

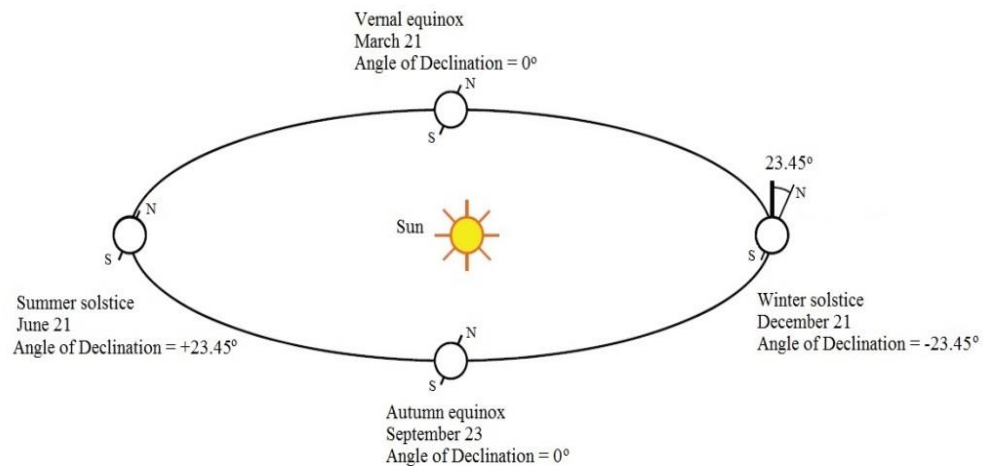


Figure 2.6. Earth's orbit around the sun and the angle of tilt in earth's axis around the year (Häberlin 2012).

Figure 2.6 depict the earth's orbital motion around the sun and tilt angle during the summer solstice, the winter solstice and the equinoxes.

2.4 Factors affecting solar radiation

Apart from position of sun and location of observation point, there are a number of factors which influences the amount of solar radiation which reaches the earth's surface. Some of these factors are reflection, absorption and scattering. The solar radiation which finally reaches earth's surface without any modification is direct solar radiation and the amount of solar radiation which is scattered, absorbed and reflected is diffused solar radiation (Pidwirny 2006). Even the direct radiation is not available in its full efficiency as some of it is reflected back from earth's surface.

This reflection from surface varies depending on different types of surfaces. It is estimated that about 51% of total global solar radiation is available for energy purposes. Remaining 49% however gets reflected, absorbed or scattered while propagating through the atmosphere. About 4% of this radiation is reflected by earth's surface. Atmosphere reflects 6% of this radiation. The reflection due to clouds amounts to 20%. The remaining 19% of this solar radiation is absorbed by clouds, aerosols and other atmospheric factors. These values are approximated for standard weather conditions and vary for different conditions. (Pidwirny 2006)

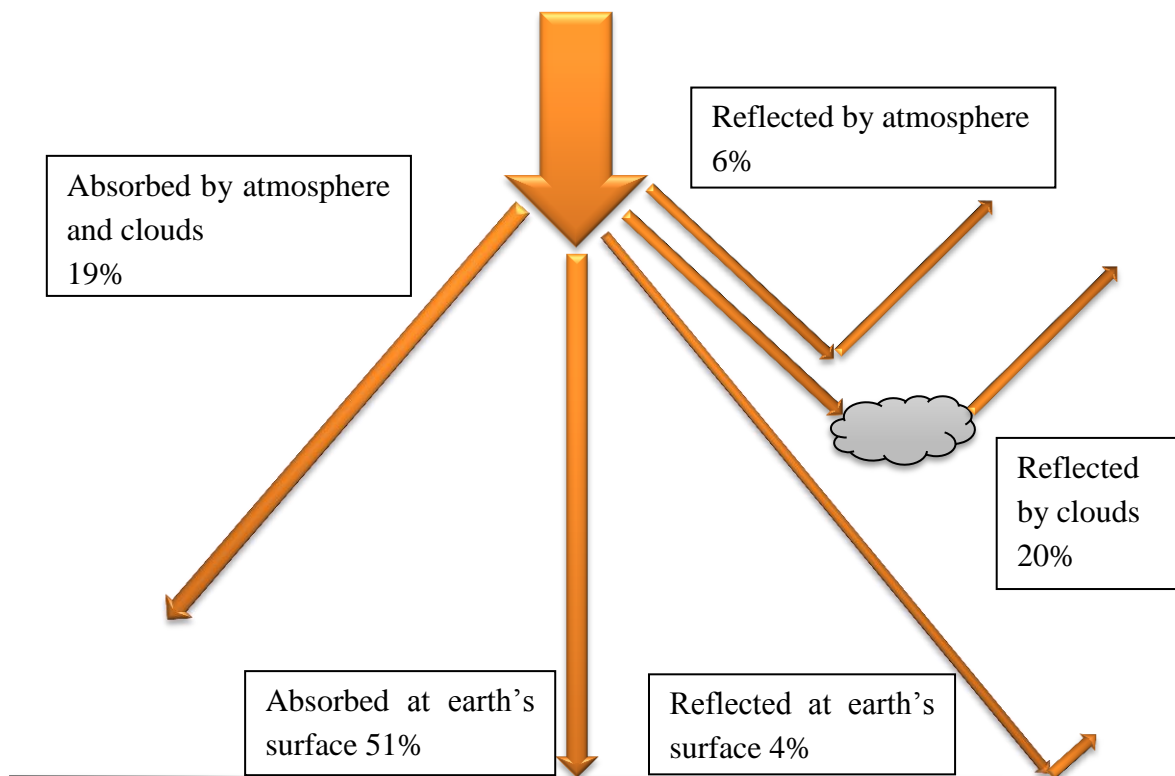


Figure 2.7. Modification in incoming global solar radiation in earth's atmosphere (Pidwirny 2006).

Figure 2.7 depict how the incoming global solar radiation gets modified when it propagates through earth's atmosphere. The processes of reflection, absorption and scattering along with estimated proportion of solar radiation are shown in the figure. These values are approximated for standard weather conditions and vary for different conditions (Pidwirny 2006).

2.5 Effects of shading

Shading is another important factor which influences the efficiency of a PV system. Partial shading is the main reason for the mismatch losses in PV systems resulting in the yield to a large extend. Partial shading can be caused either by clouds, physical obstacles like trees, buildings or by soiling and accumulation of dirt in the PV module. Shading factors are given importance while designing performance of a PV system. The main difficulty in measuring shading is that its position moves according to motion of sun and same is the case of clouds. (Lappalainen 2013) The characteristics between PV power output and PV voltage for shaded conditions is given below.

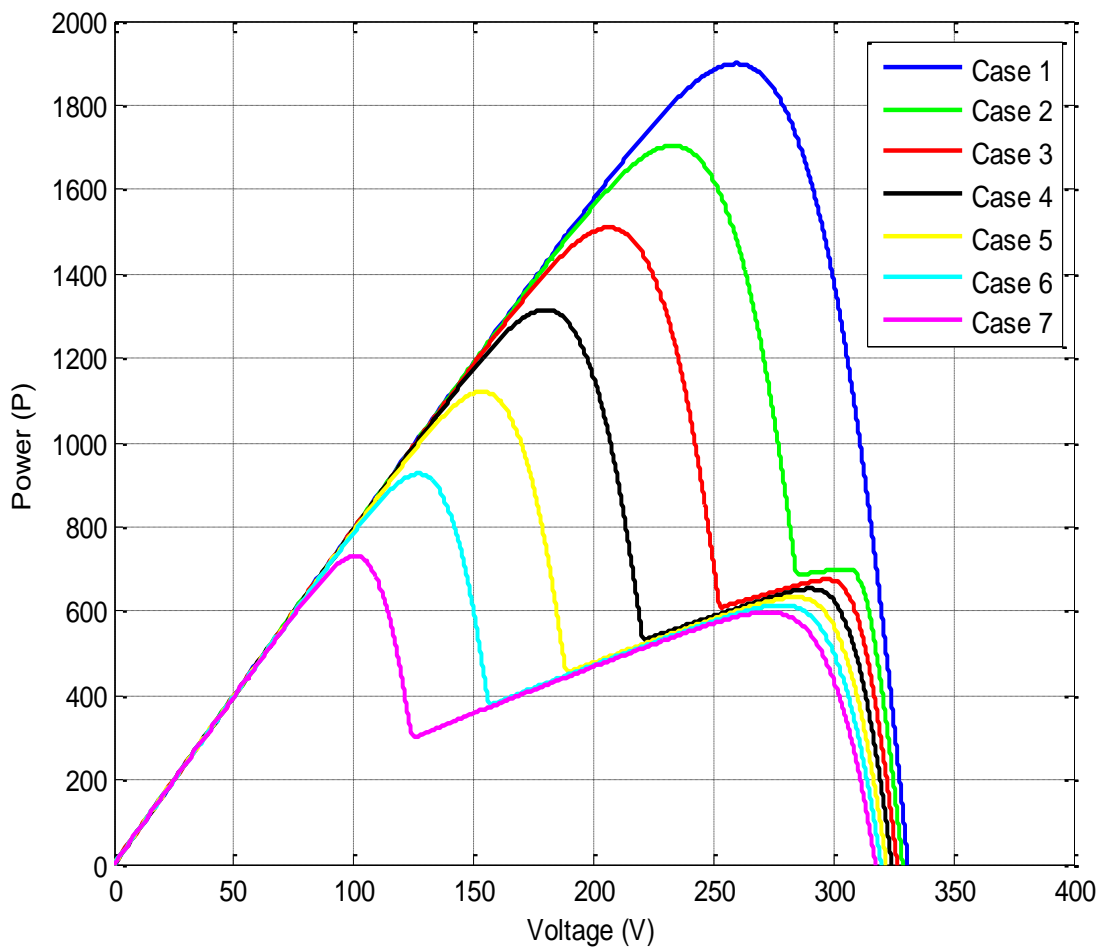


Figure 2.8. PV characteristics of a series connected string of 7 PV modules under partial shading conditions (Lappalainen 2013).

Figure 2.8 depicts PV characteristics of a series connected string of 7 PV modules under partial shading conditions in PV modules. Here a PV system with seven PV modules is studied. In case 1 there is no shading effect. In case 2 a single module is partially shaded. Similarly in remaining cases 2, 3, 4, 5 and 6 modules are shaded respectively. The input power of unshaded modules is 1000 W/m^2 and shaded modules are 300 W/m^2 during test conditions. The difference in power output during these shading conditions is shown in the figure. The power decreases as the number of partially shaded PV modules increases in the system. The effects of shading can be minimized by carefully planning and selecting location to implement the PV system. The location should be selected such that the chances of shading due to physical objects are low.

3. DIFFUSE RADIATION

Diffuse radiation is part of global solar radiation which reaches the earth's surface after getting scattered by different particles present in the earth's atmosphere. This chapter describes about diffuse radiation and primary reasons for diffusion in the atmosphere.

3.1 Introduction

Diffuse radiation is produced as a result of scattering in the atmosphere. Scattering can be caused due to suspended particles, aerosols and other components present in the atmosphere. The amount of solar diffuse radiation varies with variation in turbidity and cloud discharges of atmosphere. Seasonal variations are also possible due to different composition of atmosphere during the seasons. The cloud discharges and turbidity varies with seasons. Also pollution level and air pollutants in atmosphere influence diffusion of solar radiation. (Bhattacharya, Kar, Bhattacharya 1996) The diffuse radiation which reaches earth's surface can be utilized for photovoltaic power production. Diffuse radiation doesn't have a particular direction like direct radiation and shadowing is lower in case of diffuse radiation compared to direct radiation due to this property (Masters 2004). The table 1 shows the rate of scattering and absorption of solar radiation in earth's atmosphere and some of the factors responsible for scattering and absorption.

Table 3.1 Rate of radiation scattering and absorption under clear sky conditions (Balafas, Athanassopoulou, Argyropoulos, Skafidas, Dervos 2010).

Factor	Scattering (%)	Absorption (%)
Ozone	0	2
Water vapour	4	8
Dry air	7	2
Upper dust	3	2
Lower dust	0	0

The rate of diffuse radiation varies from place to place depending on the climatic conditions prevailing in the respective place of study. In most conditions the diffuse radiation is pretty equally distributed in the atmosphere. Thus diffuse radiation is most efficiently harvested when the solar panels are set in a horizontal manner. Increasing the tilt angle of solar panels will result in loss of diffuse radiation. When the tilt angle of solar panels is reduced to 45°, they collect up to 75% of solar diffuse radiation and remaining 25% is lost. It is also estimated that optimum tilt angle would be almost similar to the latitude of location where the panels are located. (Masters 2004)

3.2 Atmospheric scattering

The earth's atmosphere interacts with the transfer of electromagnetic radiations like solar radiation in different ways depending on the wavelength of the radiations. The radiations gets reflected, scattered or absorbed. As we study about diffuse radiation scattering phenomenon is more relevant to this paper. Reflection, refraction and diffraction are various forms of scattering in atmosphere. The earth's atmosphere is composed of various gases like nitrogen, oxygen and many other gases. The gaseous interactions and other particle components in atmosphere catalyze the scattering of incoming solar radiation. The particle size also determines the scattering process and thus there are different scattering phenomena classified on the size of particles causing it.

3.2.1 Rayleigh scattering

Rayleigh scattering is used to term the scattering process in atmosphere which takes place due to presence of particles which are smaller when compared to wavelength of incoming solar radiation. Rayleigh in the late 19th century made an approximation for the cross section of smaller, dielectric, spherical particles compared to the wavelength of incoming solar radiation. (Sneep, Ubachs 2005) The equation is as follows

$$\sigma = \frac{32\pi^3}{3\lambda^4 N^2} (n - 1)^2, \quad (3.1)$$

where N is density of molecule and λ is wavelength of incoming solar radiation (Sneep, Ubachs 2005). Some examples of Rayleigh scattering are the scattering of incoming solar radiation by gas atoms of nitrogen and oxygen present in the atmosphere. The blue sky effect is most common phenomenon caused by Rayleigh scattering. Here the incident solar light is scattered down to earth but the amount of scattering is higher at the blue end of the spectrum which results in a blue sky. The red end of the spectrum is less scattered and thus here scattering at blue end of spectrum with a wavelength of 400 nm is much higher than scattering at red end of spectrum at 700 nm. This proves that Rayleigh scattering is highly dependent on the wavelength of the incoming solar radiation and also causes enhancement of shorter wavelengths of light. (Young 1981) Rayleigh also calculated the intensity of the scattering by formulating an equation

$$I = I_0 \left(\frac{8\pi^4 N \alpha^2}{\lambda^4 R^2} \right) (1 + \cos^2 \theta), \quad (3.2)$$

where α is the polarizability which is a dimensionless size parameter, R is the distance from scatterer, θ is the scattering angle and I_0 is initial intensity. Another important factor about Rayleigh scattering is that, it is a kind of elastic scattering where there is no loss of photon energy. The total energy before scattering and after scattering remains the same. Hence there is no energy absorbed by the scatterer during the process. (Hahn 2009)

3.2.2 Mie scattering

Mie scattering is used to define the scattering of incident white light by particles of larger diameter in the atmosphere. Here the larger particles in atmosphere scatter all components of radiation in an equal manner unlike the Rayleigh scattering. The clouds in the sky appears white to the observer as a result of this scattering by larger particles in the atmosphere. Mie scattering is not largely dependent on wavelength of incoming solar radiation and also produces white light through scattering by mist and fog. Also mie scattering occurs mostly at lower layers of atmosphere where the larger particles are in abundant. The main factors which cause mie scattering in the atmosphere are aerosols, hail, clouds and rain particles. (Hahn 2009) According to mie theory the cross sections of differential scattering are given as

$$\sigma_{vv} = \frac{\lambda^2}{4\pi^2} i_1, \quad (3.3)$$

where σ_{vv} is vertical cross section, λ is the wavelength and i_1 is the intensity function. The horizontal cross section for differential scattering is given by the equation

$$\sigma_{hh} = \frac{\lambda^2}{4\pi^2} i_2, \quad (3.4)$$

where σ_{hh} is horizontal cross section and i_2 is the intensity function. For an unpolarized light the cross section of differential scattering can be calculated by calculating the average for the above equations

$$\sigma_{scat} = \frac{\lambda^2}{8\pi^2} (i_1 + i_2), \quad (3.5)$$

where σ_{scat} is cross section for differential scattering of unpolarized light. (Hahn 2009)

The natural factors which cause mie scattering include cloud, hail and rain particles in the atmosphere. Aerosols are one of the most common particles which cause mie scattering in the atmosphere. They are classified into different types based on their scattering and absorption effects such as direct effect aerosols. The color and composition of aerosol particle affects its scattering properties to large extend. The light, translucent and bright colored aerosols tend to reflect the light whereas the dark colored aerosols tend to absorb the light. The aerosols comprised of nitrates and sulphates nearly reflect all the radiation it encounters. The aerosols comprised of black carbon nearly absorb all the radiation it encounters. So aerosol scattering is highly dependent on color and composition. (Chin, Diehl, Ginoux, Malm 2011)

3.3 Clearness and Clear sky index

The idea of comparing radiation values to maximum clear sky value potential was first introduced in the year 1954 by Black et al. In this method the ratio daily radiation values to maximum radiation under clear sky conditions were calculated to develop standard equation to calculate daily sunshine hours available. Years later in 1960, two scientists Liu and Jordan gave the modern interpretations for the concept of clearness index. They formulated coefficients K_T , K_d and K_D which represented ratio of measured values of global radiation, diffuse radiation and direct radiation over extraterrestrial radiation. The term clearness index is also referred to as cloudiness index and is interchangeable. (Engerer, Mills 2014)

Clearness index can be defined as the ratio of measured irradiance to extraterrestrial irradiance at a given location (Cristina 2010). Clearness index can be calculated in hourly, daily and monthly basis. Clearness index can be calculated by equation

$$K_t = \frac{G_h}{I_0 \epsilon \sin \alpha}, \quad (3.6)$$

where G_h is global radiation on horizontal surface, I_0 is extraterrestrial radiation, ϵ is eccentricity correction factor of earth's orbit and α is the altitude angle (Cristina 2010).

The clearness index was evolved into much efficient clear sky index in the year 1981 by two scientists Bird and Hulstrom (Engerer, Mills 2014). Since then clear sky index has been used in most of modern PV systems. Clear sky index is used to estimate the cloud coverage in a given location. Clear sky index is alternate way to measure the amount of light attenuated by the atmosphere in hourly, daily or monthly period. The clear sky index can be represented mathematically as

$$K_c = \frac{\text{Measured clear sky}}{\text{Calculated clear sky}}, \quad (3.7)$$

alternatively the cloudiness of the sky can be measured by $(1 - K_c)$. (Marty, Philipona 2000).

Instruments like hemispheric sky imagers which are automatic have been used to measure cloud coverage despite being delicate and expensive for storing large amount of data. Another technology used for clear sky index measurement is broadband short wave measurements which measures the ratio of clear sky diffuse radiation to clear sky global radiation. The main drawback for this method is that it allows detection of cloud only during the day time. Also clear sky measurements depend largely on the longwave irradiance from the atmosphere along with humidity and temperature readings above the ground.

3.4 Measurement of solar radiation using empirical models

This chapter deals with measurement of diffuse radiation on horizontal and inclined surfaces.

3.4.1 Based on sunshine hours

The empirical models mostly use the Angstrom - Prescott model for estimating global solar irradiance. The Angstrom – Prescott equation is given as

$$\frac{G_P}{G_O} = a + b \left(\frac{n}{N} \right), \quad (3.8)$$

where G_P is monthly mean of average daily solar irradiance on a horizontal surface, G_O is the monthly mean of average daily extraterrestrial radiation on a horizontal surface, a and b are location specific coefficients, n is the monthly mean daily sunshine hours and N is the maximum number of monthly mean daily sunshine hours. (Prescott 1940) G_O is given by the equation

$$G_O = \frac{86400}{\pi} I_O \left(\frac{\pi}{180} \omega_s \sin\varphi \sin\delta + \cos\varphi \sin\omega_s \right), \quad (3.9)$$

where I_O is the solar constant, φ is the latitude of location, δ is the solar declination, ω_s is the angle of mean sunrise hour. Solar declination δ , can be calculated using the equation

$$\delta = 23.45 \sin \left[\frac{360 (K+284)}{365} \right], \quad (3.10)$$

where K is the number of days starting from January 1st. ω_s can be calculated from the equation

$$\omega_s = \cos^{-1}(-\tan\varphi \tan\delta), \quad (3.11)$$

3.4.2 Based on air temperature

Global solar irradiance can be also measured using empirical model based on air temperature. According to Hargreaves and Samani (1982), clearness index can be calculated using the equation

$$\frac{G_P}{G_O} = \alpha (\Delta T)^{0.5}, \quad (3.12)$$

where ΔT is the temperature difference between mean value of daily maximum temperature and daily minimum temperature. α is a dimensionless factor which is influ-

enced by altitude. Allen (1995) proposed a model to study the influence of altitude on α which is as follows

$$\alpha = \alpha_a \left(\frac{P}{P_0} \right)^{0.5}, \quad (3.13)$$

where P and P₀ are the pressure at the location of study and at sea level respectively. α_a has a fixed value of 0.17 for continental regions and 0.20 for coastal regions Allen (1995).

In 2005, Chandel, Aggarwal and Pandey proposed a different model

$$\frac{G_P}{G_0} = 7.9 \varphi^{-1} \left(\Delta T \sin \varphi \left(\frac{P}{P_0} \right) \right)^{0.5}. \quad (3.14)$$

In this model α_a is expressed in terms of latitude φ and is given as

$$\alpha_a = 7.9 \varphi^{-1} (\sin \varphi)^{0.5}. \quad (3.15)$$

In these models it is important to estimate the values of a and b with respect to the location of study for maximum accuracy Allen (1995).

3.5 Direct measurement of solar radiation

The direct and diffuse radiation reaching earth's surface can be measured using a number of devices. The most commonly used devices for measuring solar radiation is as follows.

Pyrheliometer is a broadband device which is used to measure direct radiation which reaches the earth's surface. The instrument has a continuous tracking system which enables it to be aimed at sun all the time. It is sensitive to radiation of wavelengths between 280 nm – 3000 nm. The basic working principle of Pyrheliometer is as follows. The radiation enters the device through a sealed single crystal quartz window which is followed by a thermopile which converts the heat produced to electric signal which is recorded and converted to equivalent energy using a calibration factor. (Tiwari, Dubey 2010)

The device has two blackened strips of manganin arranged such that one strip is exposed to sun and the other is shaded. Each strip has a connected thermopile and can be electrically heated. The shaded strip is heated by an electrical signal so that the temperature between the strips remains the same, so that the electrical energy to shaded strip is equal to solar radiation absorbed by the exposed strip. Then the product of incident solar radiation, strip area and absorptance is equated to the supplied electrical energy to determine solar radiation. A second value can be determined by interchanging the strip functions using a movable shutter. This allows the measurements to be more accurate

by eliminating edge effects and lack of uniformity in electrical heating. (Tiwari, Dubey 2010) A CHP1 pyrheliometer is shown in figure 3.1.



Figure 3.1. CHP1 Pyrheliometer (Kipp & Zonnen 2015).

Pyranometer is another common device used for measuring solar radiation. Pyranometer is an actinometer which can measure broadband of solar radiation on a planar surface. The device also consists of sensors to measure solar radiation flux density in a 180° field view. The working principle is almost similar to that of pyrheliometer but the sensitive surface here is exposed to solar radiation which is also reflected from surface and other surrounding structures. A multijunction, circular thermopile is used as a sensor in pyranometers. The cold junction is electrically insulated and the temperature variation between hot and cold junction is used as a function of solar radiation absorbed. The sensitive surface is covered by two glass domes to protect it from wind and rain. When a pyranometer is supplemented by a shading ring it can be used to measure the diffuse radiation. (Tiwari, Dubey 2010)

Pyranometers measure solar radiation on a horizontal surface and thus any tilt in the angle can cause an error in the reading. The voltage reading from the sensors is converted to energy units by using appropriate calibration factor. Radiation data is usually integrated over a period of time like hours to days. Solar cell pyranometer is another type of pyranometer used for radiation measurements. The main drawback of this device is that the spectral response is not linear, thus making system calibration as a function of spectral distribution. A typical pyranometer is a passive device which does not require any input power. ISO 9060 standardization is used to standardize pyranometer and this system is also adopted by World Meteorological Organization (WMO). Calibration of pyranometers is done relative to World Radiometric Reference (WRR) which is maintained by World Radiation Center (WRC) in Switzerland. (Tiwari, Dubey 2010) A CMP21 pyranometer is shown in figure 3.2.



Figure 3.2. *CMP21 Pyranometer (Kipp & Zonnen 2015).*

Sunshine recorders are another commonly used device used to measure solar radiation. The measurements are used to understand climate of the area and is of importance to fields of science, tourism and agriculture. The basic types of sunshine recorders use sun itself as measure of time of occurrence of event and the other one uses a time scale. In earlier sun shine recorders the interpretation of results by an observer was required. But in modern sunshine recorders, due to use of computers and electronics does not require the observer's interpretation. A sunshine recorder is shown in figure 3.3. (Tiwari, Dubey 2010)



Figure 3.3. *Sunshine recorder (Lomb 2011).*

Also the new devices can measure global and diffuse radiations. The device consists of a glass ball mounted on brass bowl with grooves holding recording cards. When exposed to sun this forms trace on recording cards. There are grooves for 3 sets of cards. The long curved for summer, short curved for winter and straight cards for the equinoxes. (Tiwari, Dubey 2010)

4. SOLAR PV RESEARCH PLANT AT TUT

This chapter gives a brief description about the solar photovoltaic research plant at Tampere University of Technology. The various components of the plant including hardware and software were researched and chosen by Diego Torres Lobera and was published in his master's thesis in 2010.

4.1 PV plant layout

The layout design of TUT solar research plant was researched briefly by Diego Torres Lobera in 2010 in his master thesis. The layout and construction of the photovoltaic plant was finalized during spring of 2010. The solar panels were connected using grid connection to support research purposes. 69 NP190GKg solar panels are used in the plant. The total nominal power value is 13.1 kW. The panels are arranged in 6 different strings to form three 6 panel strings and three 17 panel strings. The panels were positioned in such a way to minimize the effects of shadowing on them at the roof. The TUT solar photovoltaic power station test plant is illustrated in appendix A.

Several different outputs for different power configurations are offered by the system. Torres Lobera (2010) suggested two different configurations in his research. The first configuration consists of three strings of 17 panels and one string of 18 panels. The second configuration consists of three strings and each consists of 23 panels. The electrical features of both configurations were also studied. The first configuration is 4-output configuration and second configuration is 3-output configuration. Table 4.1 shows the electrical features of 4-output and 3-output configurations.

Table 4.1 Electrical features of 4-output and 3-output configurations (Torres Lobera 2011).

4-output configuration		3-output configuration	
17-panel string		23-panel string	
P_{MPP}	3.2 kW	P_{MPP}	4.4 kW
U_{MPP}	440 V	U_{MPP}	596 V
U_{OC}	563 V	U_{OC}	563 V
18-panel string			
P_{MPP}	3.4 kW		
U_{MPP}	466 V		
U_{OC}	596 V		

4.2 Sensors

The automatic weather station installed in TUT uses a number of sensors to measure different climatic parameters. This chapter briefly describes the sensors used in the automatic weather station and its use. Climatic measurement system at TUT is used to measure the parameters which can affect the performance and efficiency of photovoltaic modules and also the solar radiation measurements which includes global, direct and diffuse radiation. The climatic measurement system consists of 69 solar panels and was built during the year 2010. It is located on the rooftop of Department of Electrical Engineering at Tampere University of Technology. The panels used in the system are from Naps Systems Oy. The model of the panels is NP190GKg. (Torres Lobera 2010)

The average temperature in Helsinki during July is 17 °C and during January is -5 °C. These values are high considering the latitude of location. These high values are caused due to warming effects of the Gulf Stream. The modules and measurement system are set to withstand and operate under extreme climatic conditions. During winter the system can operate under -25 °C and even under no sunlight at all. During summer the system can operate at temperatures above 25 °C and around irradiance levels of 1000 W/m². (Torres Lobera 2010) Figure 4.1 shows the solar research plant photovoltaic module arrangement on roof top.



Figure 4.1. Section of TUT solar PV power station test plant.

The system has a number of sensors for measuring various climatic variables. The data from the sensors are transmitted to sensor cables and then to SF/UTP cables. The sensor data then travels to the data logger inside the Department of Electrical Engineering building. (Ahola 2011) Table 4.2 gives a list of sensors and the manufacturer used in the measurement system for different climatic variables.

Table 4.2 Sensors used for measuring various climatic variables in automatic weather station (Ahola 2011).

Climatic Variables	Sensors used	Manufacturer
Solar irradiance on the modules	SP LITE2	Kipp & Zonen
Global irradiance	CMP22	Kipp & Zonen
Diffuse irradiance	CMP21 with CM121C shadow ring	Kipp & Zonen
Temperature & Humidity	HMP155	Vaisala
Wind speed	WS425	Vaisala

4.2.1 Solar irradiance on PV modules

The automatic weather station is installed with a SP LITE2 sensor to measure the power received by the solar panel modules. It is manufactured by Kipp & Zonen. The sensor can be used under all weather conditions. The unique design of diffuser in the sensor gives it an excellent directional response and the sensitivity is proportional to cosine of incident angle of radiation, creating an accurate and consistent measurements. The sensor is also self-cleaning in nature. (Ahola 2011)

SP LITE2 sensor can produce measurements in 180° angle of view. A direct reading in power units can be obtained by dividing measured voltage by the calibration factor of the sensor. The calibration factor for the sensor is set by the manufacturer. The sensor consists of adjustment screws and a mounting flange which is bubble level integrated for convenience of use. A high quality Kipp & Zonen yellow cable is connected to the sensor. (Ahola 2011) A SP LITE2 sensor is shown in figure 4.2.



Figure 4.2. Solar irradiance sensor SP Lite2.

4.2.2 Diffuse and global irradiance

A CMP21 sensor is installed in the automatic weather station to measure the diffuse radiation. The sensor is manufactured by Kipp & Zonen. It is high performance research grade pyranometer. It is compliant with ISO 9060 secondary standards. The sensor measures the irradiance on a planar surface. The sensor has excellent linearity and fast response time. The operational temperature range is between $-40\text{ }^{\circ}\text{C}$ – $+80\text{ }^{\circ}\text{C}$ which makes it operational under the weather conditions in Finland. The housing temperature is monitored by a standard thermistor sensor. The sensor also has a redesigned sun shield covering the connector. Pyranometer supplies a low voltage of $0 - 20\text{ mV}$ in accordance to the incoming solar radiation and thus do not require any input power. The sensor also contains a water proof socket which is also connected to the yellow signal cable. The cable is connected to a water proof plug. (Ahola 2011)

The sensor is connected with a CM121C shadow ring to measure the diffuse radiation. The shadow ring shields the sensor from direct radiation of sun. There is also possibility of interception of small parts of diffuse radiation by the shadow ring and hence correction is required to compensate for this. The shadow ring is adjusted every few days because of the change in elevation of sun every day. During initial instalment the shadow ring requires a north-south aligning, tilting of the sliding bars and shadow ring sling bar setting. The initial two settings are one time installations but the third setting requires periodical adjustments. (Ahola 2011) Figure 4.3 shows a CMP21 sensor with a CM121C shadow ring.



Figure 4.3. CMP21 pyranometer with CM121C shadow ring measuring diffuse radiation.

The automatic weather station is installed with a CMP22 sensor to measure the global irradiance. The sensor is manufactured by Kipp & Zonen. It is compliant with ISO 9060 secondary standards. The sensor has similar features to CMP21 but with few exceptions. The sensor has a high quality quartz dome which gives it a wider spectral range, reduced thermal offset and an improved directional approach. The optical quality of the sensor is high and thereby reduces the error below 5 W/m^2 . (Ahola 2011) Figure 4.4 shows a CMP22 sensor used to measure global irradiance.



Figure 4.4. CMP22 pyranometer measuring global radiation.

4.2.3 Temperature and humidity

HUMICAP HMP155 is the sensor which is used to measure temperature and humidity in automatic weather station. It is a sensor with both temperature and humidity probes and thus measures both parameters. It is manufactured by Vaisala. The sensor is designed to be stable and withstand harsh environments. The sensor has a solid probe and is shielded with a Teflon filter in order to protect it from liquid water dust and dirt. It is difficult to get accurate measurements in humid and saturated environments but the sensor has warmed probe where the sensor head is continuously warmed and thus the humidity level inside stays below ambient value thereby giving accurate measurements. This also brings down the risk of condensation on probe. The sensor has 180RC thin film polymer sensor for measuring humidity and resistive platinum sensor, Pt100 for measuring temperature. (Ahola 2011) Figure 4.5 shows HMP155 sensor arranged inside the radiation shields.



Figure 4.5. Temperature and humidity sensor HMP155 inside DTR503A and DTR502A radiation shields.

The sensor is active sensor and has a voltage range from 0 – 10 V. The humidity is scaled between 0 – 100 % and temperature is scaled between $-40 - 60$ °C with respect to the voltage range. A chemical purge is used to heat up the sensor to 180 °C in order to evaporate the interfering chemicals. The whole process takes place in 6 minutes and during this the outputs are locked. The sensor probes are installed in side DTR502A and DTR503A radiation shields in order to shield them from solar radiation and precipitation. This increases the lifetime of the sensor. DTR502A is a 9-plate radiation shield and is used with additional thermal sensor. DTR503A is a 12-plate radiation shield and is used with humidity sensor. The radiation shields are maintenance free. The radiation shields have an outer white surface which reflects the radiation and an inner black sur-

face which absorbs the accumulated heat. The sensor is recommended to be calibrated once year but it is done time to time depending on the application. Serial line connection or the buttons on the probe can be used for the calibration. (Ahola 2011)

4.2.4 Wind speed and direction

WINDCAP ultrasonic wind sensor WS425 is used for measuring wind speed and direction in the automatic weather station. It is manufactured by Vaisala. The sensor is a maintenance free and heated sensor. The average time between failures is estimated as 26 years. The sensor material is made up of stainless steel and it has large transducer heads which are insensitive to rain. In addition to this the sensor is insensitive to effects of pressure, humidity and temperature. The sensor requires very low maintenance and can be tested in case of deterioration in measuring accuracy. (Ahola 2011) Figure 4.6 depicts WS425 ultrasonic wind sensor on roof top of TUT.



Figure 4.6. Wind sensor WS425

The sensor is installed on the roof top at the highest point such that there are no other objects surrounding it. It is also connected with a lightning rod to protect the device and the personnel's. The sensor operates in analog mode. The wind speed and wind direction are measured as a function of voltage. When output voltage is 0 V, the wind speed is 0 m/s and when voltage is 1 V, wind speed is 55.88 m/s. The measurements can be also measured as function of frequency between the ranges of 0 – 625 Hz. For wind direction the output voltage of system is set from 0 to 4 V to increase the accuracy of measurements. In case of wind direction the 0 V represents 0 ° and for reference voltage 4 V the value is 360 °. (Ahola 2011) Figure 4.6 depicts WS425 ultrasonic wind sensor on roof top of TUT.

5. RESEARCH AND ANALYSIS

This chapter deals with a study conducted to learn the variations in radiation profiles and its analysis. In this chapter we study parameters influencing radiations and causing the variations. The aim of the chapter is to study the annual, seasonal and daily variations in global and diffuse radiation. It was important to analyse the effects of climatic parameters like cloudiness and humidity on the radiation profile to the research.

5.1 Annual radiation profiles

Although energy from sun is almost constant throughout the year, the irradiance value varies throughout the year. The variation of solar radiation which reaches the earth's surface varies largely due to change in the atmospheric conditions and position of the sun. These changes in solar irradiance can be visible both on a daily and yearly basis. Figure 5.1 represent the annual global and diffuse radiation profile for 2014. The location of study is Tampere University of Technology, Tampere, Finland.

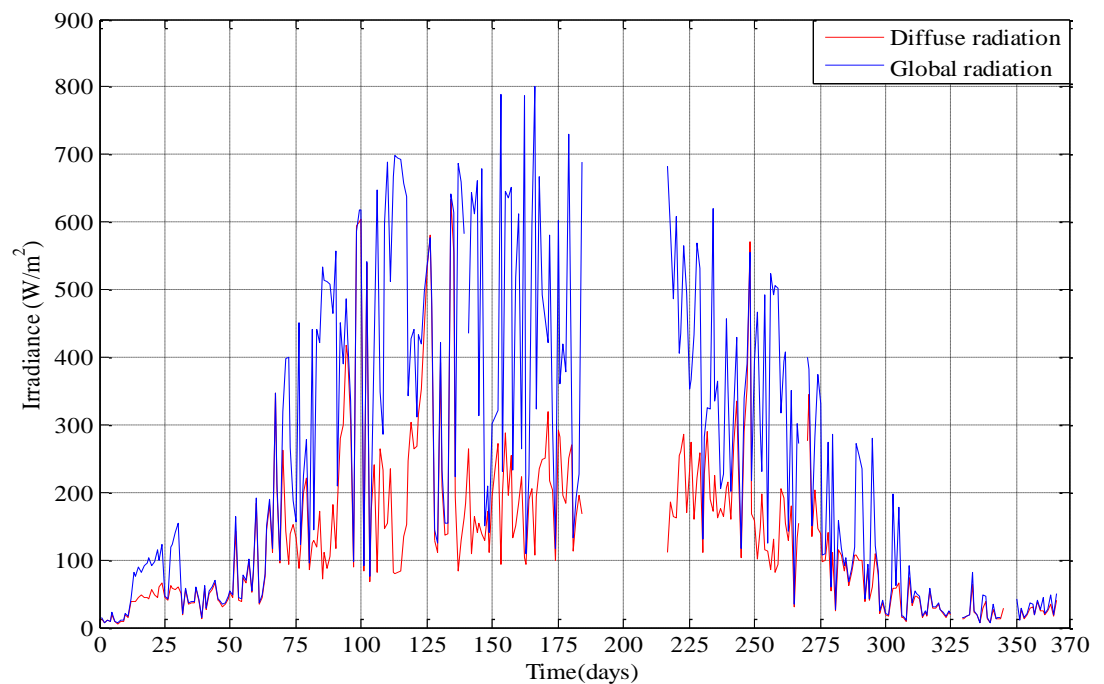


Figure 5.1. Annual radiation profile in Hervanta, Tampere for average daily values during 2014.

Some irradiance data are missing in the figure 5.1 due to system maintenance. The figure shows the variation in irradiance level, both global and diffuse radiation throughout the year.

The readings were taken between timings 10 – 14 with a time interval of 10 minutes. Average value for each day was computed using SQLfetch operation and the graph was plotted using these average daily values. The timeline was maintained for every day. From the figure we can see that during the months of January and February the irradiance level received are low and diffuse and global radiation are almost similar during most of the days. The factors which influence these variations would be the lack of sun light, snow depth, cloudiness and humidity. From mid-March the radiation levels starts rising and there is a visible difference between diffuse radiation and global radiation. The global radiation profile values are much higher than the diffuse radiation profile values from mid-March to mid-October. The radiation values reach the maximum value during the month of June. During November and December the irradiance values goes below 100 W/m^2 and this is due to the onset of winter. The maximum global irradiance value reaches up to 800 W/m^2 around the year.

For studying the annual variation in irradiance levels the global and diffuse radiation profile for 2012, 13 and 14 were studied. This study was in order to verify whether the variation in the irradiance profile follows the same pattern throughout these 3 years. Both global and diffuse radiation profiles were formed separately and compared. Some data was unavailable due to system maintenance. Figure 5.2 represent annual global irradiance profile comparison for 2012, 13 and 14. The readings were taken between timings 10 – 14 with a time interval of 10 minutes. Then the average value for each day was calculated using SQLfetch operation and graph was plotted.

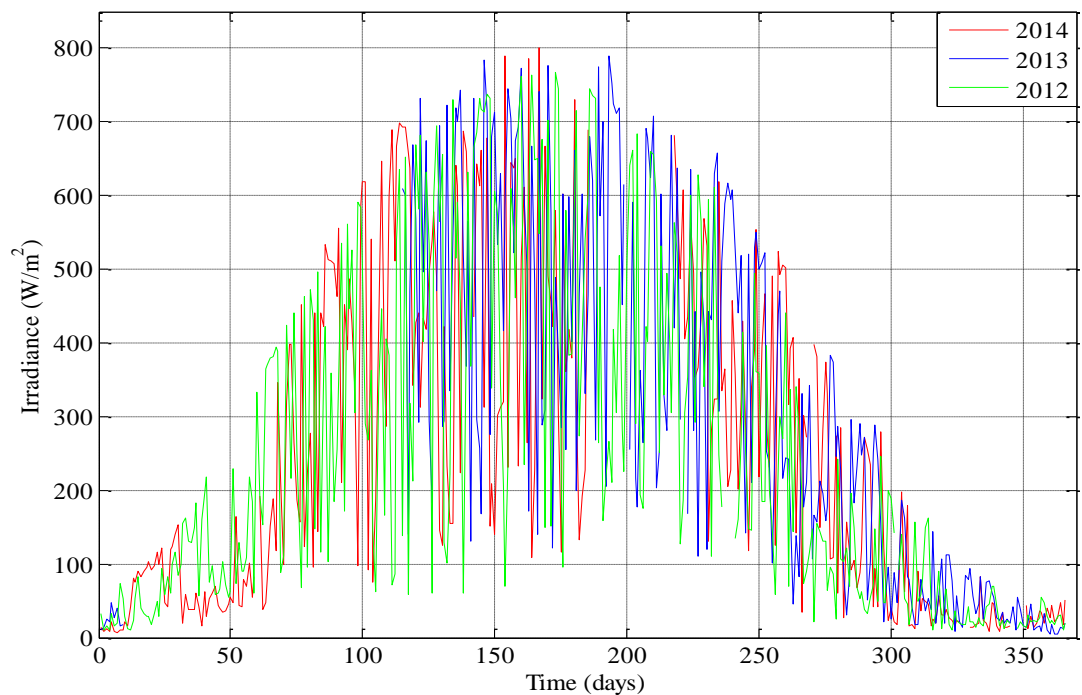


Figure 5.2. Annual global radiation profile comparison using average daily values in Hervanta, Tampere during 2012, 13 and 14.

From figure 5.2, we can study that even though there is slight variations in the profiles the pattern almost remains same throughout the 3 years. The radiation levels reach maximum value during the months of June and July and are lowest during the cold months of November and December. Figure 5.3 is a comparison for diffuse radiation profile for 2012, 13 and 14.

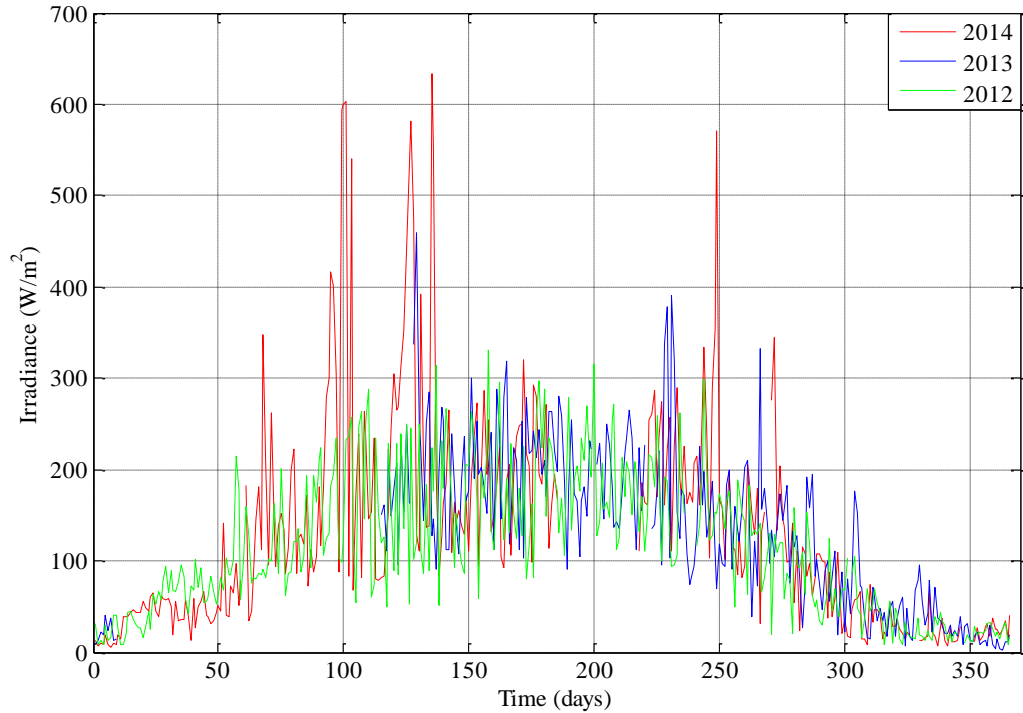


Figure 5.3. Annual diffuse radiation profile comparison using average daily values in Hervanta, Tampere during 2012, 13 and 14.

The diffuse radiation profile comparison shows us variations in the patterns for the 3 years. Unlike the global radiation profile, here we can see variation in the values on a large scale. The diffuse radiation values spikes up to around 625 W/m^2 in 2014 which is much higher compared to values of 2012 and 13. This variation is possible outcome of measurement error due to disoriented shadow ring position. These factors are studied in detail in upcoming sections.

5.2 Seasonal variation of radiation profiles

This chapter is used to study how the radiation profile varies in test location, during summer and winter. To study variations during summer August 2014 was selected as it is one of the warmest months of the year and for winter February 2014 was selected as it is one of the coldest month of the year in Finland. (Infopankki 2014) The readings were taken between timings 5:00 – 17:00 with a time interval of 10 minutes. The average value for each day was computed using SQLfetch operation and graph was plotted. Figure 5.4 represent the irradiance profile for August 2014.

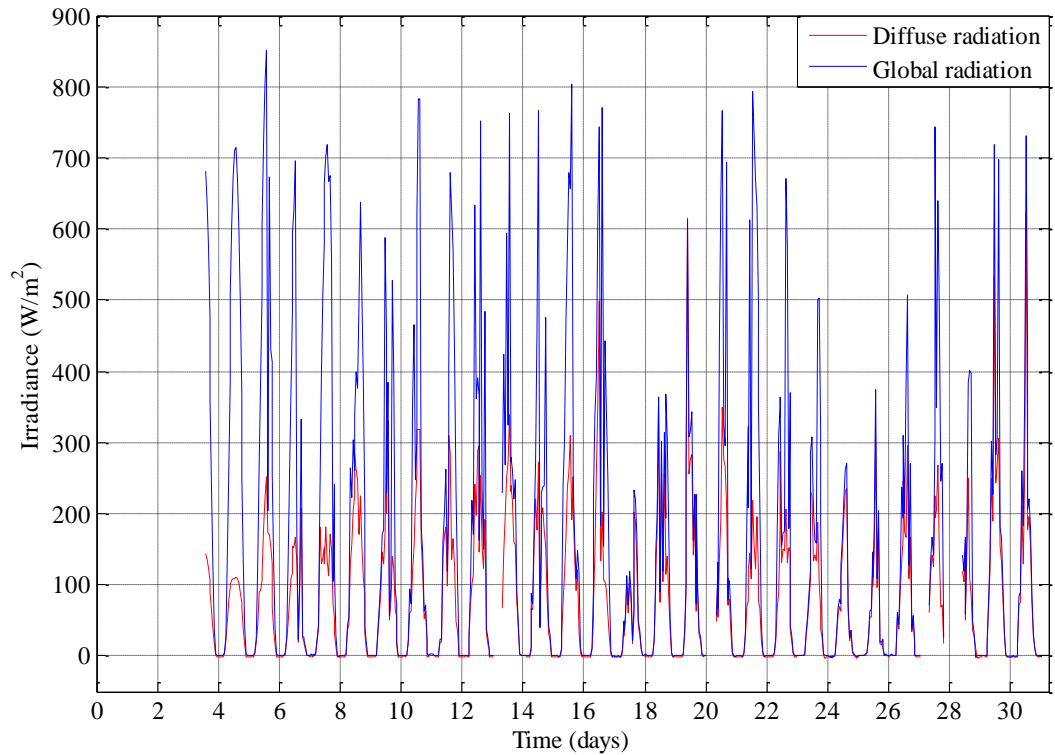


Figure 5.4. Irradiance profile for average daily values during August 2014 in Hervanta, Tampere.

Some data are missing due to system maintenance. The radiation values are higher during summer due to longer daylight hours (Infopankki 2014). The global radiation reaches up to a value of 852 W/m^2 and diffuse radiation reaches up to 622 W/m^2 . The global radiation values are much higher compared to diffuse radiation values during summer. The influence of climatic parameters like cloudiness and humidity are discussed in upcoming sections. Figure 5.5 represent the irradiance profile for February 2014.

February is one of the coldest months of the year in Finland. The daylight hours are shorter and there is snow falls (Infopankki 2014). These are some of the factors which influence the irradiance profile during cold winter months. The radiation values are much lower compared to warm summer months. The highest value of global radiation throughout the month is 176 W/m^2 and diffuse radiation is 159 W/m^2 . Another important characteristic is that the ratio of diffuse radiation to global radiation is much higher and closer to unity when compared to summer months. Thus rate of diffusion is higher during winter compared to summer.

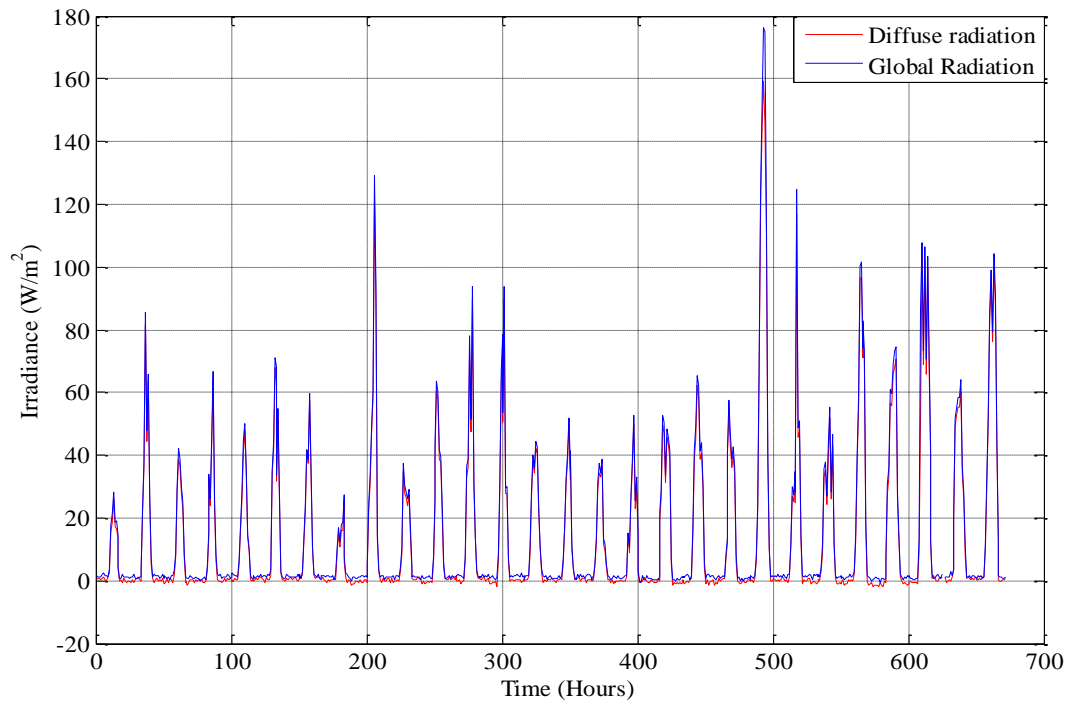


Figure 5.5. Irradiance profile for average daily values during February 2014 in Hervanta, Tampere.

Also the Global and diffuse radiation profile for each month were compared separately. Figure 5.6 represent the comparison of global radiation profile for February and August 2014.

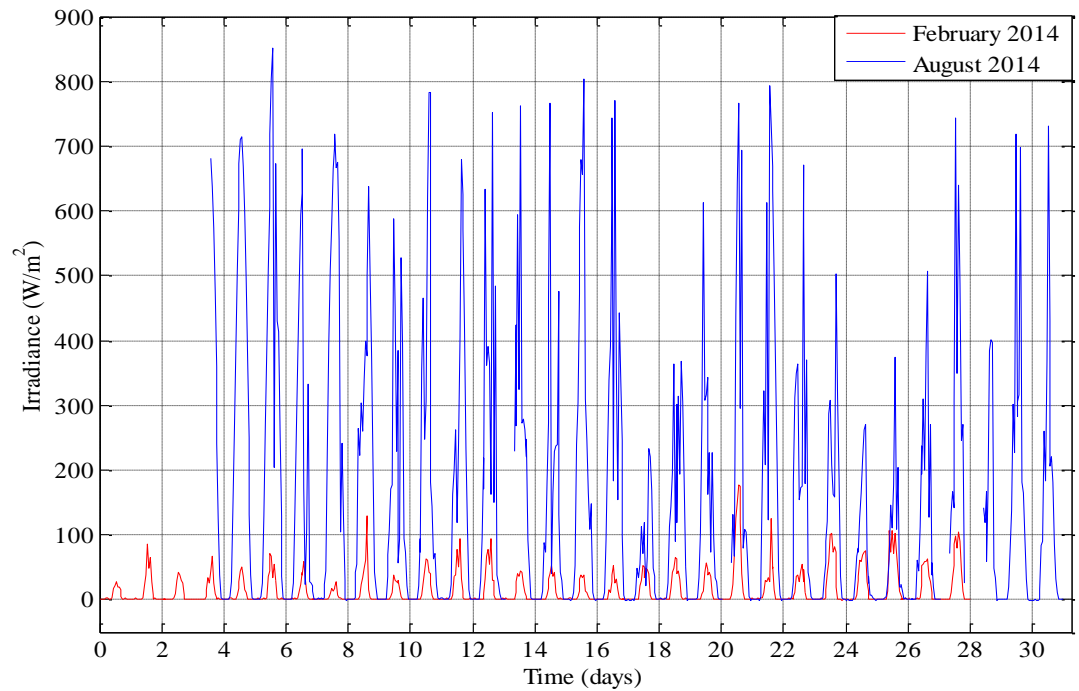


Figure 5.6. Global radiation profile comparison for average daily values during February and August 2014 in Hervanta, Tampere.

The global irradiance profile values differ greatly during February and August 2014. This value for August is much higher compared to values during February. The better daylight hours, clear sky, lower humidity and lack of snow are some of the parameters which create this variation (Infopankki 2014). Figure 5.7 represent diffuse radiation profile comparison for February and August 2014.

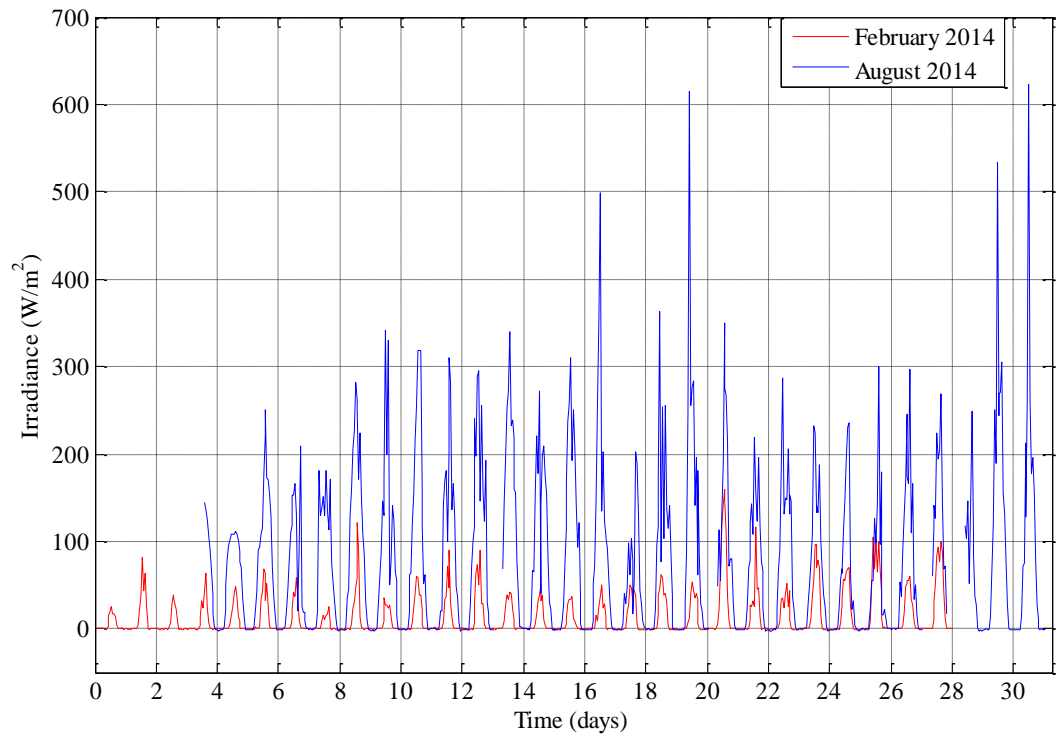


Figure 5.7. Diffuse radiation profile comparison for average daily values during February and August 2014 in Hervanta, Tampere.

As discussed above there is a large variation in diffuse radiation profile during February and August 2014. Better daylight hours are one of the main factors which create this variation.

5.3 Daily variation of radiation profiles

In order to analyse the influence of clouds on radiation profile daily variation in radiation profiles were studied. 5th and 8th August 2014 were selected to study the daily variation in radiation profile. The readings were taken for whole day with a time interval of 10 minutes. Figure 5.8 represent the radiation profile for August 5th. The radiation profile has a uniform curve with very few variations. The radiation profile has a uniform curve suggesting lack of cloud and a clear sky. To confirm this assumption cloud percentage measurements for August 5th was studied (World weather online 2015). The results for cloud percentage were supporting the assumptions made about the clear sky day. Figure 5.9 represent cloud percentage for August 5th. The cloud percentage meas-

measurements were taken from 2:00 – 23:00. The average value for every three hours was used in the graph.

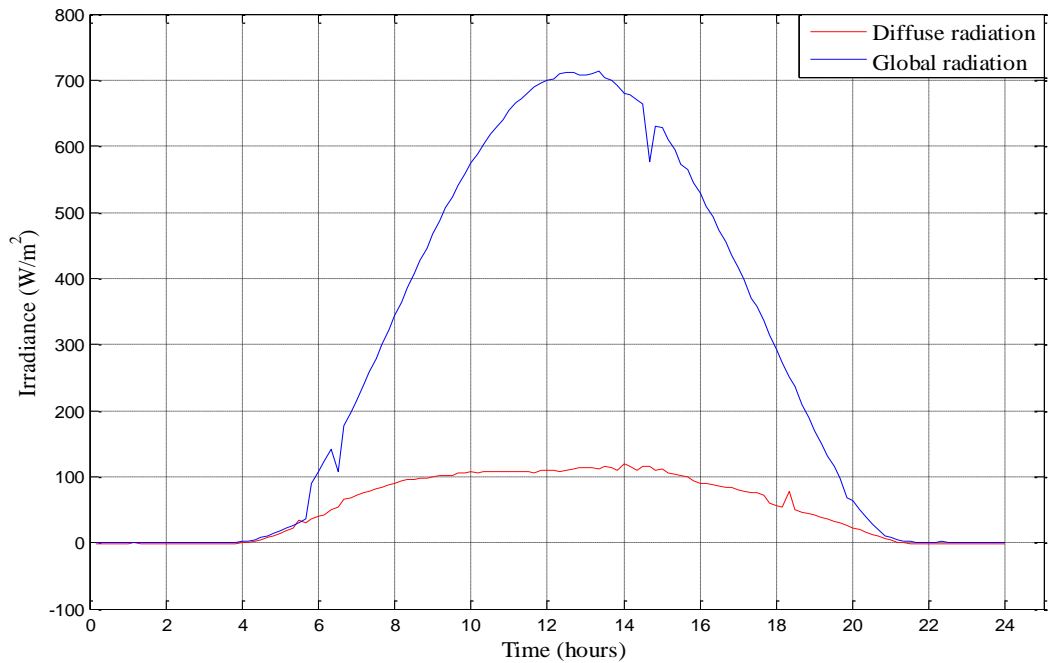


Figure 5.8. Radiation profile for clear sky day on August 5th, 2014 in Hervanta, Tampere.

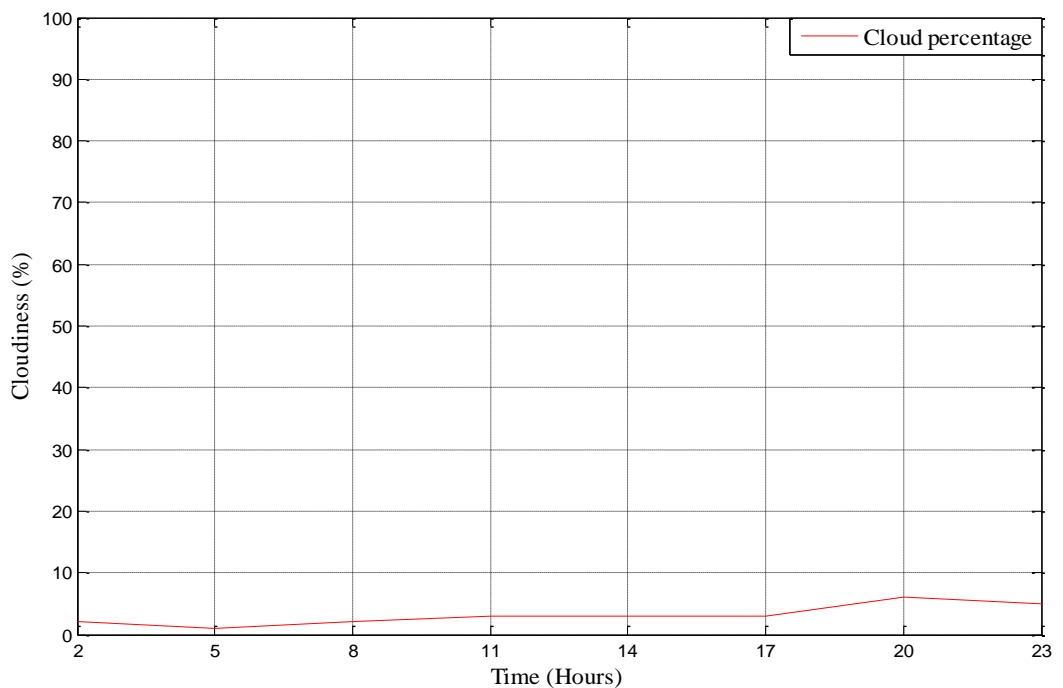


Figure 5.9. Cloud percentage profile for August 5th, 2014 in Hervanta, Tampere.

The cloud distribution for august 5th shows us that it was a clear sky day and maximum amount of cloud was 6 % on that day. Figure 5.10 represent the radiation profile for

August 8th. The radiation profile has a large number of variations suggesting a cloudy day. The diffuse radiation values are also much higher compared to August 5th. The cloud percentage measurements were studied to validate this assumption. Figure 5.11 represent cloud percentage for August 8th. The cloud percentage measurements were taken from 2:00 – 23:00. The average value for every three hours was used in the graph.

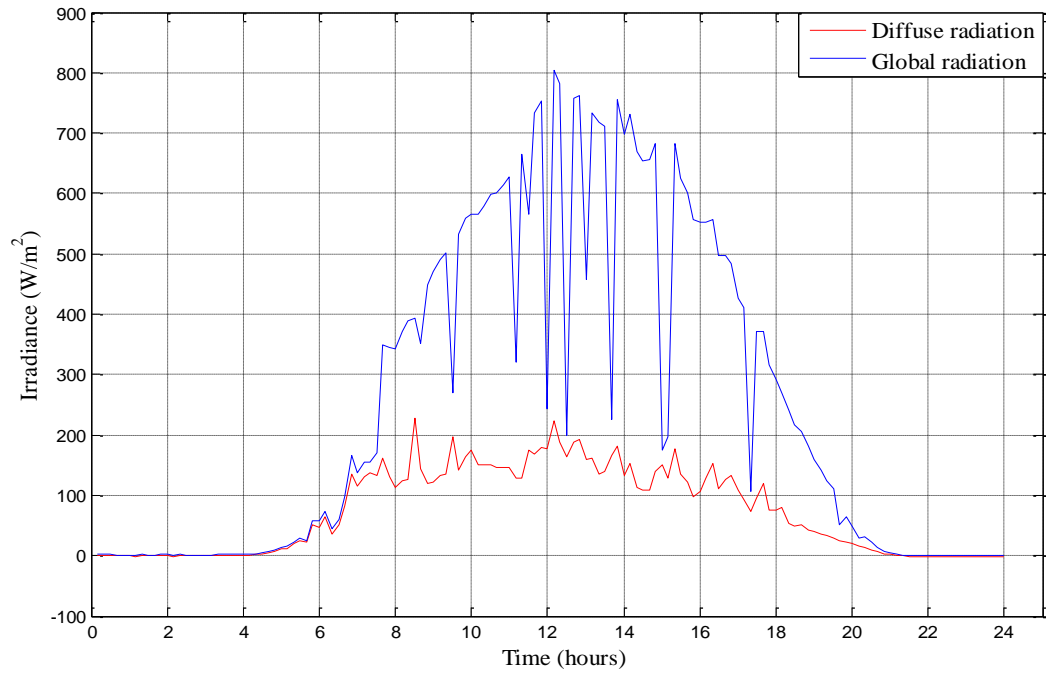


Figure 5.10. Radiation profile for cloudy day on August 8th, 2014 in Hervanta, Tampere.

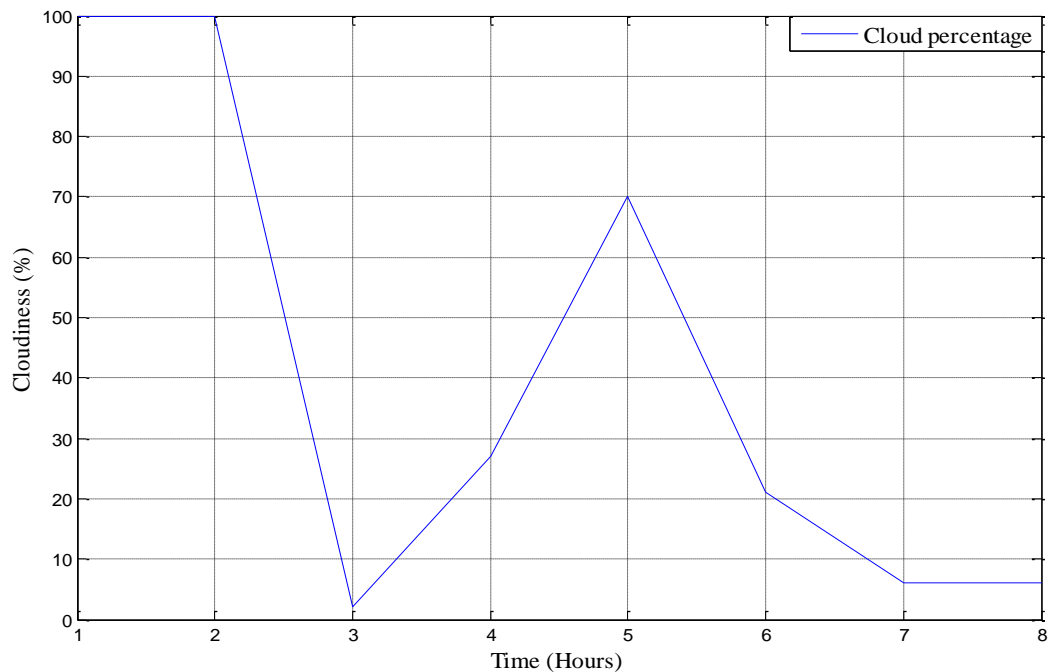


Figure 5.11. Cloud percentage profile for August 8th, 2014 in Hervanta, Tampere.

The cloud percentage profile suggest that the earlier assumptions of August 8th being a cloudy day. The cloud percentage is high throughout the day reaching up to 100 %. The humidity variations were also compared for the both days to study the effects of humidity on irradiance profile. Figure 5.12 represent comparison of humidity during the test days.

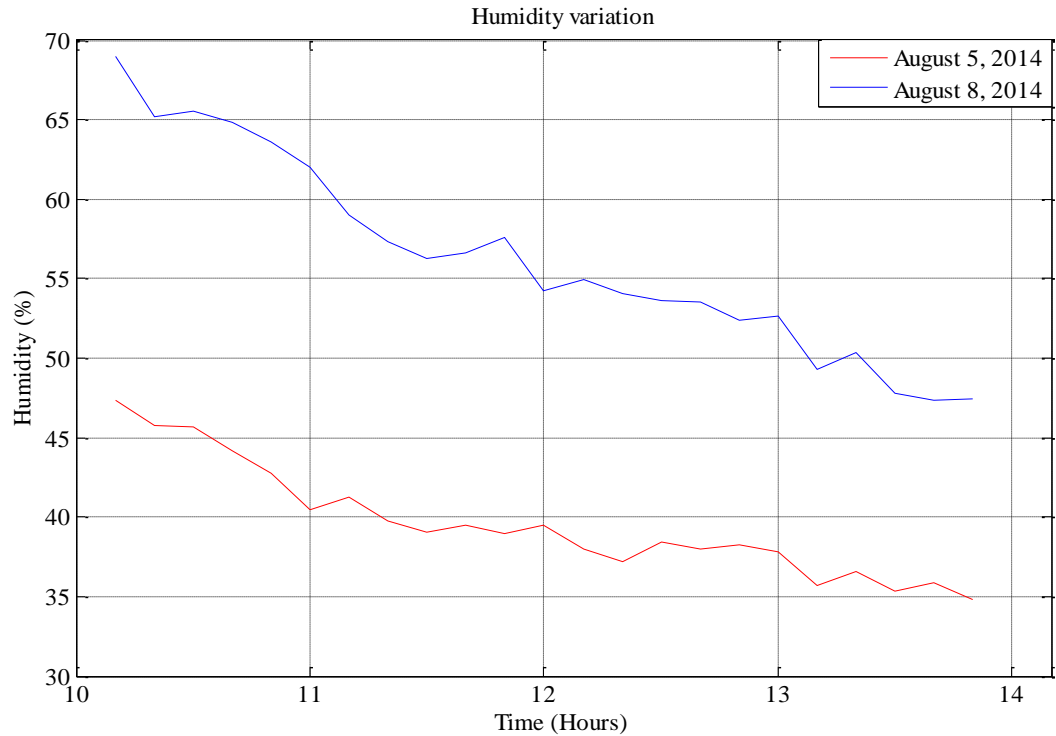


Figure 5.12. Humidity comparison profile for test days August 5th and 8th, 2014 in Hervanta, Tampere.

The humidity percentage was measured from 10:00 – 14:00 with a time interval of 10 minutes. The humidity values during August 8th are much higher compared to August 5th. The profile suggests that the amount of diffuse radiation increases with increase in humidity content in the atmosphere.

5.4 Irradiance ratio and cloud distribution

From previous sections it was evident that the irradiance profiles dependent on the cloud distribution. So in order to have a deeper understanding the ratio of diffuse radiation to global radiation was compared to cloud percentage over August 2014. The readings were measured every 10 minutes from 5:00 to 20:00 and average for each day was calculated. The average daily value of diffuse radiation was compared to average daily values of global radiation. The ratio of irradiance values were then plotted to average daily cloud percentage value from 5:00 to 20:00. Figure 5.13 represent irradiance ratio and cloud percentage graph.

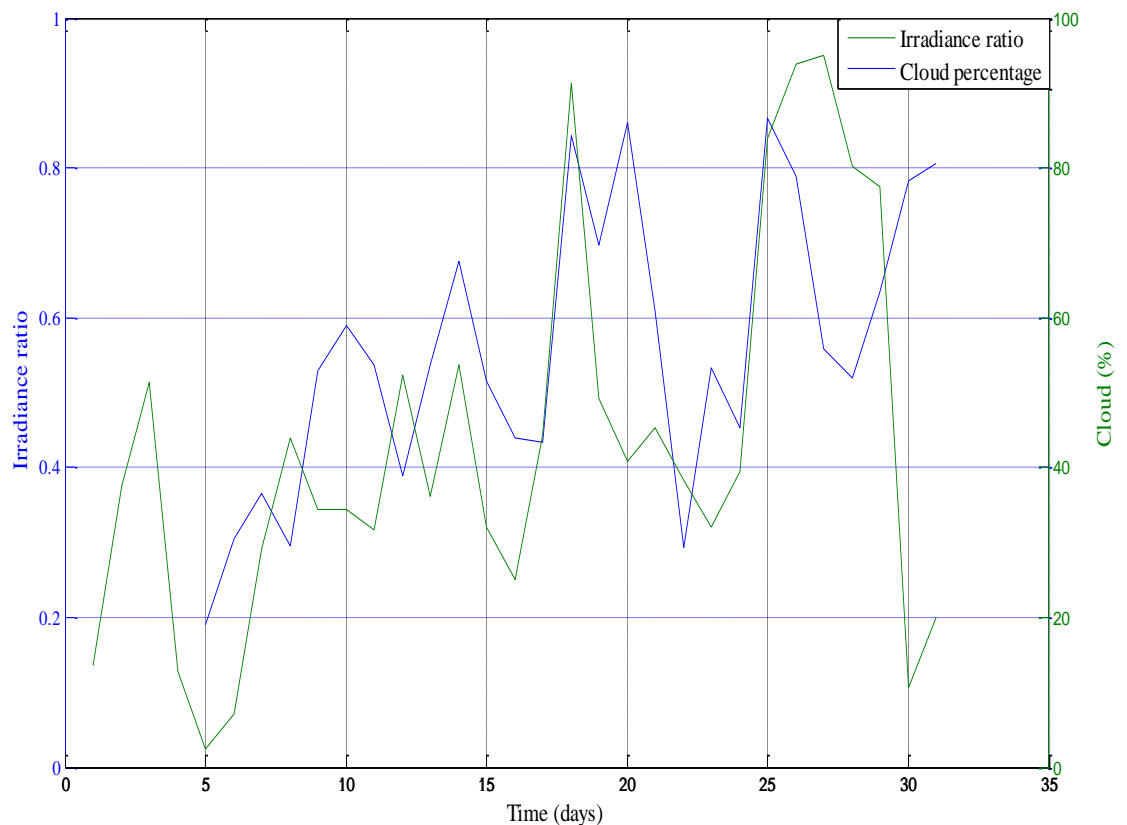


Figure 5.13. Average daily ratio of diffuse and global irradiance and cloud percentage during August, 2014 in Hervanta, Tampere.

From the figure we can see the irradiance ratio has a higher value when the cloud percentage is higher. This characteristic is almost uniform throughout the month. Thus we can infer that the value of diffuse radiation is higher during cloudy days. Some measurements are missing due to system maintenance.

5.5 Irradiance ratio and humidity

The variation of irradiance profile with humidity of atmosphere was also noted during the research. The influence of humidity on irradiance profile was studied. The irradiance ratio values were measured. The humidity values were measured using HMP155 sensor. The humidity values were measured at a time interval of 10 minutes from 5:00 - 20:00 over August 2014. The average daily values were then calculated and plotted with irradiance ratio values. Figure 5.14 represent characteristic graph for relationship between humidity and irradiance ratio. From the figure we can see that the irradiance ratio is increase with rise in humidity percentage. The pattern is almost followed throughout the month. Thus the humidity of atmosphere plays a major role in rate of diffuse radiation.

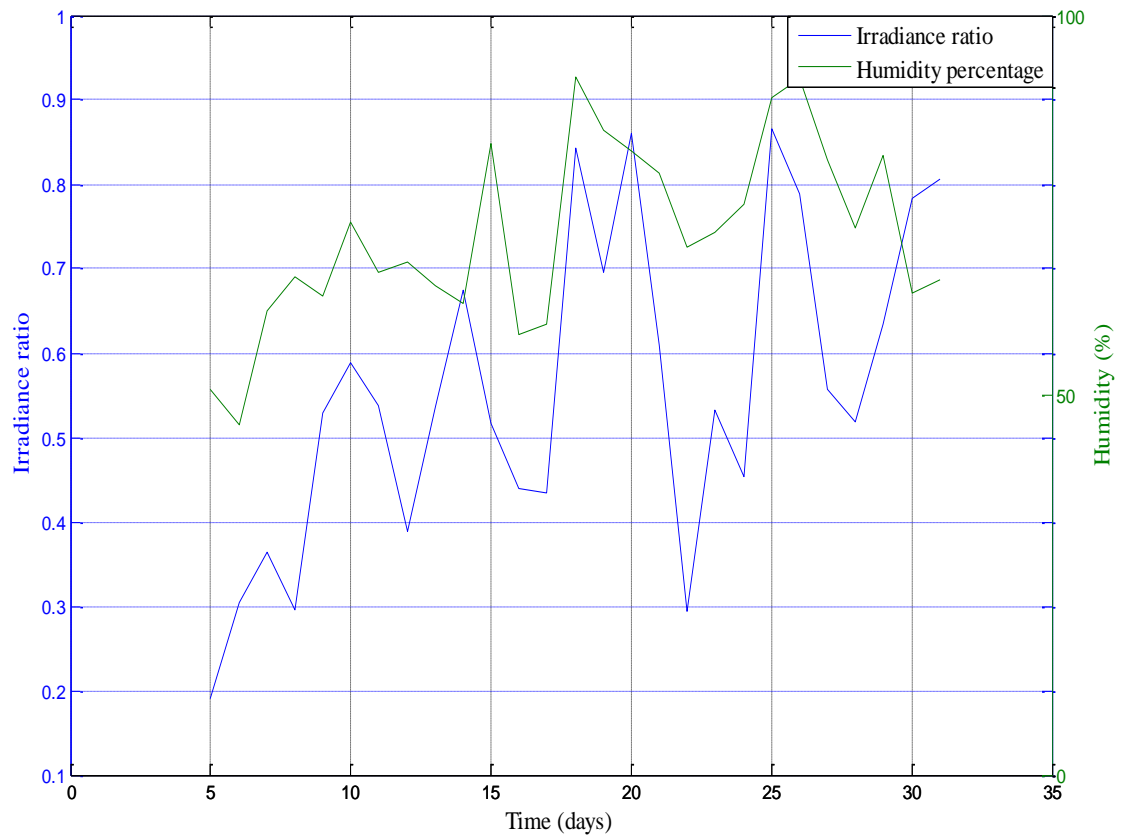


Figure 5.14. Average daily ratio of diffuse and global irradiance and humidity percentage during August, 2014 in Hervanta, Tampere.

6. CONCLUSIONS

From the previous chapter we studied how the irradiance profile varies annually. The diffuse radiation has a major role in operation of photovoltaic power plants. The absorption and scattering in the atmosphere causes power loss in solar irradiance. Diffuse radiation causes change in spectral content of the solar radiation. The increase in humidity and presence of clouds and other air borne structures can increase the amount of diffuse radiation. During the research the annual variation in diffuse radiation was studied in detail. The ratio of diffuse radiation to global radiation was found to be higher during the winter months in Finland. The aim of thesis was to study how the annual irradiance profile varies. In order to study the annual variations in radiation profiles the global and diffuse radiation measurements for over 3 years were studied. In all those analysis the diffuse radiation value was almost same as global radiation ratio during the winter months. The daylight hours are shorter during winter. Thus the efficiency of photovoltaic power plant is decreased due to higher amount of diffuse radiation.

The variation of radiation profile with climatic parameters was also studied during the research. The cloud variation was one of the factors which influenced the irradiance profile. The ratio of diffuse radiation to global radiation was higher whenever the cloud percentage was higher. This indicates the efficiency of power production decreases on cloudy atmospheric conditions due to increase in rate of diffuse radiation. During clear sky conditions the ratio of diffuse to global radiation is lower. Thus during these atmospheric conditions global radiation values are high and the power production in photovoltaic power plant is more efficient. Humidity variation was another important factor which influenced the radiation profile. During the research it was found that with increase of humidity level in the atmosphere the diffuse to global radiation ratio was higher.

During the analysis of measurements it was found that the diffuse radiation affects the working of photovoltaic power plant. The efficiency of photovoltaic power plant decreases with increase in rate of diffuse radiation. The climatic parameters like cloud and humidity content of atmosphere cannot be altered. The seasonal analysis of radiation profile showed that the overall amount of radiation was higher during months of June, July and August due to extended day light hours and minimum during December, January and February due to shortened day light hours. Thus during winter months it is important to harvest available radiation for maximum power production and efficiency. The appropriate method to increase the efficiency of photovoltaic power plants during these conditions is to modify it in such a way that diffuse radiation is harvested and converted to power. Direct radiation is collected at higher efficiency when the solar

panels are tilted in a way such that the radiation hits them at a 90° angle. But diffuse radiation is collected effectively by solar panels when they are positioned in a horizontal manner. Thus for maximum working efficiency of photovoltaic power plants it is important to adjust the tilt angle of solar panels periodically according to different seasons. The results of the study indicate that solar irradiance in Finland is low during half of the year and thus it is important to harvest both global and diffuse radiation during this time to ensure maximum power production and working efficiency.

REFERENCES

- [1] Ahola, J. Photovoltaic research power plant measuring and data storing system. Master of Science Thesis. Tampere University of Technology. Tampere 2013, pp. 3–34.
- [2] Allen, R. Evaluation of procedures for estimating mean monthly solar radiations from air temperature. Food and Agricultural Organisation of the United Nations. Italy 1995.
- [3] Baker, E., Fowlie, M., Lemoine, D. and Reynolds, S. S. The economics of solar electricity. Energy Institute at Haas. USA 2013, pp. 2–10.
- [4] Balafas, C.A., Athanassopoulou, M.D., Argyropoulos, T., Skafidas, P. and Derivos, C.T. Effect of the diffuse radiation on photovoltaic inverter output. National Technical University of Athens. Greece 2010, IEEE. 1 p.
- [5] Bhattacharya, A. B., Kar, S. K. and Bhattacharya, R. Diffuse solar radiation and associated meteorological parameters in India. European Geosciences Union. 1996, pp. 1051–1059.
- [6] Chin, M., Diehl, T., Ginoux, P. and Malm, W. Intercontinental transport of pollution and dust aerosols: implications for regional air quality. Atmospheric chemistry and physics vol. 7, 2007, pp. 5501–5517.
- [7] Chou, M. D., Suarez, M.J. A solar radiation parameterization for atmospheric studies. Technical report series on global modelling and data assimilation vol. 15, NASA. 1999, pp 1–14.
- [8] Cristina, Ș. Estimating clear sky global radiation using clearness index, for Brașov urban area. 3rd International Conference on Maritime and Naval Science and Engineering. Romania 2010, pp. 150–153.
- [9] Engerer, N.A. and Mills, F. P. K_{PV} : a clear-sky index for photovoltaics. Solar energy vol. 105, 2014, Elsevier. pp. 679–693.
- [10] Fthenakis, V. M. 2003. Overview of potential hazards. Practical Handbook of Photo voltaics: Fundamentals and Applications 1st ed. Elsevier. UK 2003, pp. 1–14.
- [11] Grover, S. Energy, economic and environmental benefits of the solar America initiative. NREL. USA 2007, pp. 21–24.
- [12] Hahn, D. W. Light scattering theory. University of Florida. USA 2009, pp. 1–13.

- [13] Hargreaves, G. H. and Samani, Z. A. Estimating potential evapotranspiration. *Journal of the Irrigation and Drainage Division* vol. 108 no. 3, 1982, pp. 225–230.
- [14] Häberlin, H. *Photovoltaics system design and practice*. Switzerland 2010, John Wiley and Sons. pp. 27–47.
- [15] Hummel, R. E. *Electronic properties of materials* 4th ed. Chapter 2. Springer science and business media, LLC. 2007.
- [16] Infopankki. Finnish climate. 2014. [accessed on 20.03.2015]. Available at: <http://www.infopankki.fi/en/information-about-finland/basic-information-about-finland/finnish-climate>
- [17] Jayakumar, P. *Solar energy resource assessment handbook*. APCTT, 2009.
- [18] KIPP & ZONEN. KIPP & ZONEN CHP 1 pyrheliometer web page. [accessed on 17.03.2015]. Available at: <http://www.kippzonen.com/Product/18/CHP-1-Pyrheliometer#.VTdy-mO8pOI>.
- [19] KIPP & ZONEN. KIPP & ZONEN CMP 21 pyranometer web page. [accessed on 17.03.2015]. Available at: <http://www.kippzonen.com/Product/14/CMP-21-Pyranometer#.VTduGGO8pOI>.
- [20] Lappalainen, K. *Effects of climate and environmental conditions on the operation of solar photovoltaic generators*. Master of Science Thesis. Tampere University of Technology. Tampere 2013, pp. 4–77.
- [21] Larsen, C., Brooks, B. and Starrs, T. *Connecting to the grid: a guide to PV interconnection issues* 3rd ed. IREC. USA 2000, pp. 4–14.
- [22] Lomb, N. *How do you catch sunshine? Use a Campbell-Stokes sunshine recorder*. Sydney observatory. 2011. [accessed on 17.03.2015]. Available at: <http://www.sydneyobservatory.com.au/2011/how-do-you-catch-sunshine-use-a-campbell-stokes-sunshine-recorder/>.
- [23] Marty, C. and Philipona, R. The clear-sky index to separate clear-sky from cloudy-sky situations in climatic research. *Geophysical Research Letters* vol. 27 no. 17, 2000, pp. 2649–2652.
- [24] Masters, G. M. *Renewable and efficient electric power systems*. 2004, John Wiley and Sons. pp. 415–416.
- [25] Pidwirny, M. *Introduction to geography. Fundamentals of physical geography* 2nd ed. 2006, 1 p.

- [26] Prescott, J. A. Evaporation from water surface in relation to solar radiation. *Transactions of the Royal Society of Australia* vol. 46, 1940, pp. 114–118.
- [27] Riordan, C.J., Hulstrom, R. L. and Myers, D. R. Influences of atmospheric conditions and air mass on the ratio of ultraviolet to total solar radiation. *Solar Energy Research Institute*. USA 1990, pp. 1–7.
- [28] Shockley, W. and Queisser, H. J. Detailed balance limit of efficiency of p-n junction solar cells. *Journal of Applied Physics* vol. 32, 1961, pp. 510–519.
- [29] Sneep, M. and Ubachs, W. Direct measurement of the Rayleigh scattering cross section in various gases. *Journal of quantitative spectroscopy and radiative transfer* vol. 92. 2005, Elsevier. pp. 294–297.
- [30] Thesis Writing Guide in English. Tampere University of Technology guidelines. Tampere. 2013. [accessed on 13.11.2014]. Available at: <https://www.tut.fi/pop> > Study info > Master's thesis > MSc % thesis guidelines.
- [31] Tiwari, G. N. and Dubey, S. Fundamentals of photovoltaic modules and their applications. Chapter 1. RSC Publishing. 2010.
- [32] Torres Lobera, D. Measuring actual operating conditions of a photovoltaic power generator. Master of Science Thesis. Tampere University of Technology. Tampere 2010. pp. 49–72.
- [33] TUT Solar PV Power Station Test Plant. Appendix A. In: Torres Lobera, D. Measuring actual operating conditions of a photovoltaic power generator. Master of Science Thesis. Tampere University of Technology. Tampere 2010, pp. 96 p.
- [34] United States Department of Energy. The history of solar. 2012. [accessed on 15.11. 2014]. Available at: https://www1.eere.energy.gov/solar/pdfs/solar_timeline.pdf.
- [35] Varró, S. A study on black body radiation: classical and binary photons. *Hungarian Academy of Sciences*. Hungary 2006, pp. 365–389.
- [36] World Weather Online. 2015. [accessed on 05.03.2015]. Available at: <http://www.worldweatheronline.com/Tampere-weather/Western-Finland/FL.aspx>
- [37] Young, T. A. Rayleigh scattering. *Applied optics* vol. 20 no. 4, Optical Society of America. USA 1981, pp. 533–535.

APPENDIX A: TUT SOLARPHOTOVOLTAIC POWER STATION TEST PLANT

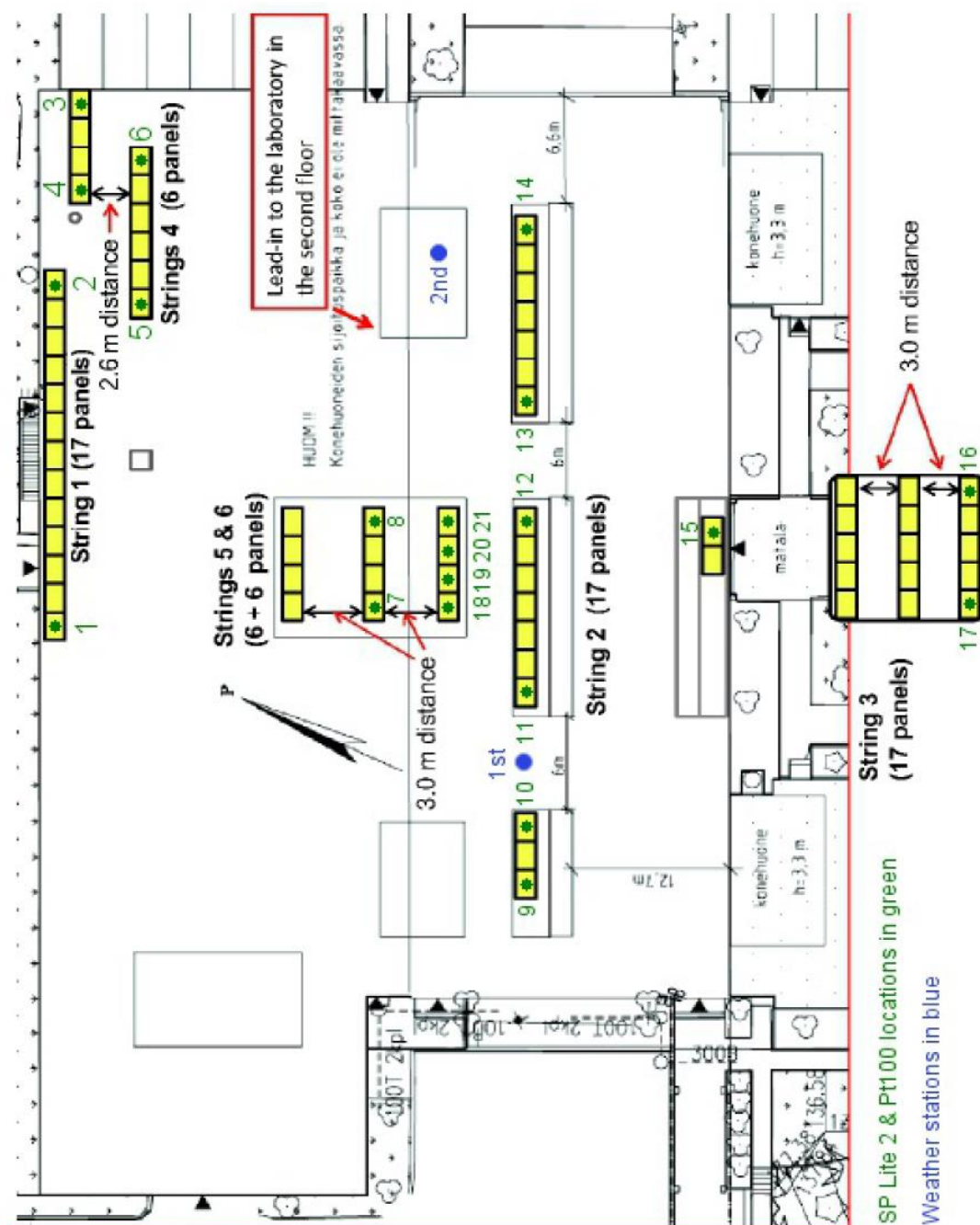


Figure A.1: TUT solar photovoltaic power station test plant (Torres Lobera 2010).